AD A139 933 THE STUDY OF AN IDEALIZED WING/BODY JUNCTION(U) VON KARMAN INST FOR FLUID DYNAMICS RHODE-SAINT GENESE (BELGIUM) G STRINGFIELD 31 MAR 84 VKI-PR 1983 2R 1/1

UNCLASSIFIED EOARD-TR-84-13 AFOSR-83-0127 F/G 20/4 NL

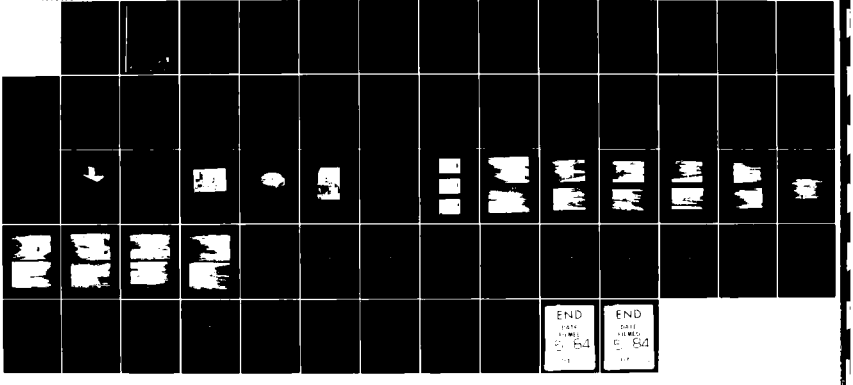

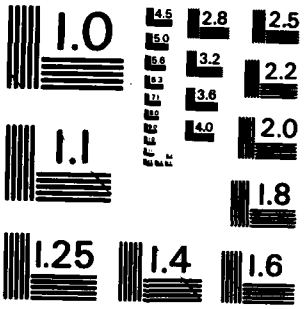

MICROCOPY RESOLUTION TEST CHART
NATIONAL BUREAU OF STANDARDS-1963-A

EOARD-TR-84-13

GRANT AFOSR 83-0127

THE STUDY OF AN IDEALIZED WING/BODY JUNCTION

GREG STRINGFIELD
VON KARMAN INSTITUTE FOR FLUID DYNAMICS
CHAUSSÉE DE WATERLOO, 72
B - 1640 RHODE SAINT GENÈSE, BELGIUM

MARCH 31, 1984

FINAL SCIENTIFIC REPORT, 30 APRIL 1983 - 31 JANUARY 1984

APPROVED FOR PUBLIC RELEASE; DISTRIBUTION UNLIMITED

PREPARED FOR

EUROPEAN OFFICE OF AEROSPACE RESEARCH
AND DEVELOPMENT/USA
FPO NEW YORK 09510

SECURITY CLASSIFICATION OF THIS PAGE (When Data Entered)

REPORT DOCUMENTATION PAGE	READ INSTRUCTIONS BEFORE COMPLETING FORM
1. REPORT NUMBER: EOARD-TR-84-13	2. GOVT ACCESSION NO: AD-A139933
3. RECIPIENT'S CATALOG NUMBER:	
4. TITLE (and Subtitle): THE STUDY OF AN IDEALIZED WING/BODY JUNCTION	5. TYPE OF REPORT & PERIOD COVERED: Final Scient. Rep., 30 April 83 - 31 Jan. 84
	6. PERFORMING ORG. REPORT NUMBER: VKI PR 1983-28
7. AUTHOR(s): Greg STRINGFIELD	8. CONTRACT OR GRANT NUMBER(s): AFOSR 83-0127
9. PERFORMING ORGANIZATION NAME AND ADDRESS: von Karman Institute for Fluid Dynamics, Chaussée de Waterloo, 72, B - 1640 Rhode-Saint-Genèse, Belgium	10. PROGRAM ELEMENT, PROJECT, TASK AREA & WORK UNIT NUMBERS: P.E. 61102F, Proj/Task; 2301/D1, Work Unit No. 166
11. CONTROLLING OFFICE NAME AND ADDRESS: European Office of Aerospace Research and Development/CA, Box 14, FPO New York 09510	12. REPORT DATE: March 31, 1984
	13. NUMBER OF PAGES: 55
14. MONITORING AGENCY NAME & ADDRESS(if different from Controlling Office)	15. SECURITY CLASS. (of this report)
	15a. DECLASSIFICATION/DOWNGRADING SCHEDULE

16. DISTRIBUTION STATEMENT (of this Report)

Approved for public release; distribution unlimited

17. DISTRIBUTION STATEMENT (of the abstract entered in Block 20, if different from Report)

18. SUPPLEMENTARY NOTES

19. KEY WORDS (Continue on reverse side if necessary and identify by block number)

Wing-body junction
Vortical wakes
Wake surveys
Wing-fuselage fairings
Drag reduction

20. ABSTRACT (Continue on reverse side if necessary and identify by block number)

An experimental study was performed to determine the influence of fairings on the reduction of drag which is produced by the wing-body junction.

The wing-body junction was represented by a wing mounted on a flat plate and the junction was contoured by placing different fairing sizes at the wing leading edge and wing trailing edge.

The purpose of the experiment was to observe the effect of the different fairing sizes on the wing-body junction aerodynamics.

DD FORM 1 JAN 73 1473 EDITION OF 1 NOV 65 IS OBSOLETE

SECURITY CLASSIFICATION OF THIS PAGE (When Data Entered)

EOARD-TR-84-13

This report has been reviewed by the EOARD Information Office and is releasable to the National Technical Information Service (NTIS). At NTIS it will be releasable to the general public, including foreign nations.

This technical report has been reviewed and is approved for publication.

ALBERT J. ROSA
Lt Colonel, USAF
Chief Scientist

JERRY R. BETTIS
Lt Colonel, USAF
Deputy Commander

VON KARMAN INSTITUTE FOR FLUID DYNAMICS
CHAUSSÉE DE WATERLOO, 72
B - 1640 RHODE SAINT GENÈSE, BELGIUM

PROJECT REPORT 1983-28 JUNE 1983

THE STUDY OF AN IDEALIZED WING/BODY JUNCTION

GREG STRINGFIELD

SUPERVISOR : M. CARBONARO

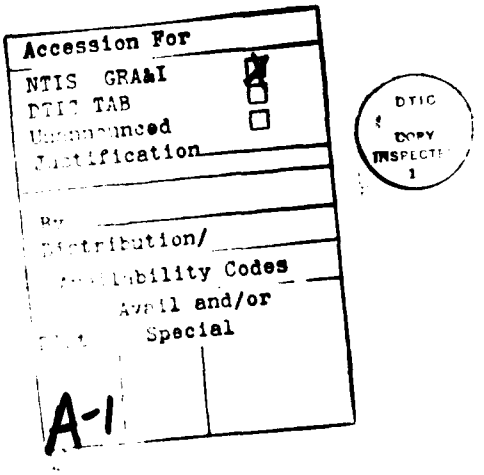

ACKNOWLEDGEMENTS

The author would like to extend a special thank you to his supervisor Mario Carbonaro for sharing his vast experience of this field of study and his knowledge of experimental techniques to greatly enhance the author's knowledge in this area of engineering.

His thanks and appreciation also go to Robert Voets and Roger Conniasselle for their willingness to assist him every step along the way.

TABLE OF CONTENTS

ABSTRACT

An experimental study was performed to determine the influence of fairings on the reduction of drag which is produced by the wing-body junction.

The wing-body junction was represented by a wing mounted on a flat plate and the junction was contoured by placing different fairing sizes at the wing leading edge and wing trailing edge.

The purpose of the experiment was to observe the effect of the different fairing sizes on the wing-body junction aerodynamics.

LIST OF SYMBOLS

α	angle of attack
b	wing span
C	wing chord
C_f	fairing chord
U_∞	free stream velocity
v	downwash velocity vector in z-direction
w	cross flow velocity vector in y-direction
X	free stream velocity coordinate
Y	spanwise coordinate
Z	coordinate perpendicular to free stream

Subscripts

∞	free stream conditions
f	fairing

LIST OF TABLES

LIST OF FIGURES

1. INTRODUCTION

1.1 Lift characteristics of wing-body combinations

The wing-body junction interference is a complex problem which is common to all aircraft, but it is unfortunately not well understood. The flow in the wing-body junction is three dimensional, subject to large pressure gradients, and difficult to measure which makes an accurate description of the flow characteristics difficult to obtain. However, the drag which is produced by the wing-body junction merits a good understanding and investigation of this flow phenomenon.

The lift characteristics of the wing-body combination can be described as an interaction of fuselage aerodynamic qualities and the wing alone aerodynamic qualities.

The fuselage, which is primarily optimized for volume, does not develop much lift due to its low aspect ratio but when it is combined with the wing the lift of the combination is improved (Ref. 1). The presence of the fuselage influences the flow around the wing by reducing the high and low pressure regions of the "wing alone" configuration. The modification of the pressure field manifests itself in the carry-over of the wing's high and low pressure regions onto the fuselage. Although the pressures are less than would be expected for the wing alone configuration, the larger chord of the fuselage will provide a larger lifting area for the pressures to act upon. Thus the wing-body combination recovers much of the lift of the wing which is inside the fuselage, but the lift of the combination is still less than the lift of the wing alone.

1.2 The problem of drag

The interference effects of a wing-body combination are largest within the wing-body junction itself (Ref. 2). These effects can be thought of as four interrelated areas of study.

The first effect induced by the junction is the displacement of the flow due to the thickness of the wing and the curved intersection lines of the wing and fuselage intersection.

Secondly, lift effects arise from the circulatory flows around the wing-body combination which are different from the lift of each individual component summed together.

Thirdly, there exists a flow asymmetry which is caused by the shape of the fuselage or the position of the wing (fore or aft of the c.g. and vertical position) on the fuselage.

Fourthly, arise the viscous effects from the viscous flow which extends along the corner formed by the intersection of the wing and fuselage.

The present experimental study examines the fourth area of the wing-body aerodynamics.

The flow approaching the wing leading edge develops a boundary layer as it travels along the fuselage. At the wing trailing edge there exists a stagnation region represented by an adverse pressure gradient which is caused by neglecting special filleting in the junction. The approaching boundary layer cannot traverse the adverse pressure gradient at the wing leading edge stagnation zone, and it will then separate from the fuselage side, rolling up into a vortex sheet or "stand-off vortex" which will shed above and below the wing-body junction (Ref. 3). The energy going into the vortex creates the drag component known as vortex drag.

1.3 The present study

The present study is an experimental investigation of the effect which fairings have upon reducing the drag which is induced at the wing-body junction. Properly designed fairings will allow the approaching boundary layer to traverse the

stagnation zone at the wing leading edge more efficiently and optimized fairings can achieve a drag reduction percentage as high as 1.5% of cruise drag (Ref. 3). Therefore, the purpose of the fairings is to guide the flow around the wing instead of allowing it to separate, roll into a stand-off vortex and hence produce energy consuming vortex drag.

This study is primarily concerned about the drag of a transport aircraft such as a Hercules C-130 aircraft which spends a great deal of its operating lifetime in the cruise flight condition at a small angle of attack. Therefore, the two primary flight characteristics, such as a turbulent boundary layer and a small angle of attack, were simulated during the tests.

The experimental study simulated a typical wing-body junction by using a model consisting of a wing mounted at a small angle of attack onto a flat plate. Section 2 describes the test setup in more detail. The wing and flat plate were then tested in a low speed wind tunnel.

Nine combinations of fairing sizes, three different sizes at the wing leading and trailing edge, were used to contour the junction. The leading edge fairings were moulded from plasticine while cardboard was used at the wing trailing edge to stay flush with the trailing edge thickness and remain fixed during the testing.

The aim of the study is to determine the influence of the fairing dimensions upon the stand-off vortex which emanates from the wing leading edge and to determine if a relationship can be found between the size of the fairing and the size and energy of the stand-off vortex which the fairings should reduce. The influence which the fairing has on the vortex can be determined by measuring the diameter of the stand-off vortex induced by each individual fairing size and by then comparing the amount of kinetic energy entrained in the vortex to illustrate

which vortices are dimensionally smaller and likewise have the least concentration of kinetic energy within them. The experimental approach applied flow visualization techniques and five-hole pressure probe measurements to complete the picture of the flow.

The flow visualization techniques involved three different methods to study the flow. Two oil flow methods were used to provide information about the flow surface streamlines and the laser light sheet method was employed to visualize the vortices and to determine their size in order to accurately determine the dimensions of the five hole traverse plane.

A five hole probe measured the pressures behind the junction to provide information about the flow quality in three aspects. The secondary flow velocities (v,w), isolines of pressure and isolines of kinetic energy were plotted to provide information and a basis for comparison of the different tests. The secondary flow plots provide a picture and a physical dimension of the vortex associated with each fairing dimension, while the isolines of kinetic energy, which is the sum of the secondary velocity components squared and divided by the free stream velocity, provide information about the amount and concentration of kinetic energy entrained in the vortex.

2. EXPERIMENTAL SET-UP AND PROCEDURE

2.1 General description

The experiments were carried out in the VKI low speed wind tunnel L-2A, at a velocity of 50 mm H_2O ($\approx$ 28 m/s). A flat plate, with a wing mounted on it, was placed horizontal in the test section and a five hole probe, mounted behind the wing, measured the pressure in one traverse plane. The data was then collected on a PET Commodore computer via a single channel transducer and a scanivalve. The velocity of the wind tunnel during the tests was monitored through a Betz manometer. An overall view of the experimental setup is shown in figure 1.

Two main objectives influenced the design of the experiment. Since the flow conditions of a transport aircraft were to be simulated, a tripper strip was placed at the flat plate leading edge to induce a turbulent boundary layer along the flat plate. At the wing leading edge the turbulent boundary layer thickness δ_T was 9.0 mm, which yields a ratio of 1:2 for the boundary layer thickness over the maximum thickness of the wing. The second point was to approximate the junction with a model comprising of a wing mounted vertically on a flat plate, which does indeed accurately model the junction as stated in reference 2. Other research such as in reference 4 illustrates the consistency and reliability of this configuration.

2.2 The experimental setup

2.2.1 The test model

The test model consists of three basic parts which are a wing, a flat plate and the fairings. The wing is a NACA 0010 symmetrical airfoil with a chord of 180 mm and painted black for oil flow visualization purposes and it is mounted on a flat plate at a 5° positive angle of attack with respect to the free stream velocity. Figure 2 provides a better view of the test model.

The fairings used in the experiment are made from plasticine and cardboard. At the leading edge, plasticine was moulded by hand into the junction and checked with a template to ensure proper dimensions. Due to the small thickness of the wing trailing edge, the trailing edge fairings were cut from cardboard and glued in place. The characteristic dimension of the fairings is the fairing chord, C_f, which ranges from 10, 20 to 30 percent of the wing chord. A total of nine combinations of fairing sizes were tested. Figures 2 and 3 illustrate the appearance and dimension of the fairings.

2.2.2 Instrumentation

The components of the data acquisition system are shown in figure 4. The principal component of the experiment is the five hole probe which is shown in figure 5. The five hole probe was chosen for its ability to measure flow angularities and because it could be manufactured very small (O.D = 2.4 mm) to accommodate a small step size during the traversing. The probe was mounted on a traverse mechanism as shown in figure 6, and connected to a Valydyne pressure transducer via a scanivalve. In order to minimize the response time of the transducer, it was placed directly adjacent to the scanivalve and connected with a small diameter tube. The transducer was calibrated using a Betz manometer as a reference.

A control drive moved the scanivalve to the desired position. At the beginning of each testing point, the operator must initialize the scanivalve to the start position. Then the scanivalve was driven through each of the five positions by the software programming.

A PET Commodore computer acquisitioned the pressure data, printed on paper and stored the data on digital cassette. The PET data acquisition system was chosen for the experiment to give an immediate indication about the faithfulness of the data while testing was in progress. The transducer could also be calibrated with ease at the beginning of each test.

Local static temperature of the tests was measured with a mercury thermometer located near the wind tunnel. Dynamic pressure or tunnel velocity was measured by the operator with a Betz manometer to an accuracy of $\pm .1$ mm H_2O, and the atmospheric pressures were measured by a mercury barometer in a nearby room.

2.3 Experimental procedure

2.3.1 Test calibration

The five hole probe was calibrated before testing began using a method developed by Wickens in reference 5, and shown in greater detail in reference 6. The method is a non nulling mode calibration technique in which probe pitch and yaw flow angles are non dimensionalized and plotted against the probe roll and pitch angles. The curves are then approximated by a polynomial expression which is fitted to the data points by coefficients. At the beginning of each test the probe was calibrated with the Commodore computer. Using the Betz manometer as reference, five known pressures were applied to calibrate the transducer signal with the Commodore computer. Since the testing was performed at 50 mm H_2O, the transducer was calibrated at that region to give the Commodore a small range with the maximum number of digits to improve the accuracy of the measurements.

After the number of digits in the Commodre was assigned to the pressure range, the Commodore was prepared to accept data from the probe. The ambient temperature and pressure were recorded in the computer and the testing could commence.

2.3.2 Test procedure

The probe was traversed manually through a traverse plane measuring 60 mm high by 110 mm wide, where the center of the plane was located at the wing trailing edge. All traverses

were performed in a plane located 1/2 C behind the wing trailing edge. The probe moved through the plane in steps of 5 mm which yields a total of 299 points in one traverse plane. The movement of the probe and the prompting of the computer were performed in the following manner. The probe was placed in position, the scanivalve initialized to the first position, the pressure indicated by the Betz manometer checked and if the tunnel velocity was correct the Commodore was prompted by the operator. The Commodore commanded the scanivalve through each of the five positions and then waited for a new prompt to repeat the process. One test lasted for approximately 2.5 hours in duration.

3. DATA REDUCTION.

A total of eleven traverses were performed, each traverse containing 299 points, and each data set followed the same flow chart as shown in figure 7. The raw data was read from the digital cassette in the PDP computer and run through a program titled JEUS which applies the coefficients from the probe calibration to the binary data so that the pressures can now be compared to the pressure values printed by the PET Commodore computer during testing. The program APPEND allows the operator to join the data sets together to build and organize the tests together into their proper format. Program UPDATE permits the operator to delete erroneous data points from the data and create the final form of the data for the plotting programs. The plotting programs are titled, JEAN, GUS and KINETIC. The first program, JEAN, calculated and plots the secondary flow velocities in the wake. Program GUS plots the isolines of pressure and KINETIC plots the isolines of secondary flow kinetic energy. The program plots the formula below

$$\frac{v^2+w^2}{U_\infty^2} .$$

These three programs produce the plots contained in this report, and those programs plotted in the PDP system on a Tektronics 4662 plotter.

4. EXPERIMENTAL RESULTS

4.1 Flow visualization

The experiment consisted of two [illegible] flow visualization. The laser sheet method was used to visualize the vortex behind the wing and to determine the dimension and location of the vortex. The size of the traverse plane behind the wing was determined after examining the results of the laser sheet visualization. Figure 8a illustrates the vortex on the under side (pressure side) of the wing at the wing trailing edge. The vortex is clearly distinguishable and exhibits a clearly defined form and composition. From this and other photographs, the traverse plane was located at 1/2 C behind the wing and it measured 60 mm high by 110 mm wide. Figure 8 illustrates the growth of the vortex and it travels downstream of the wing. Note that pictures 8b and 8c show the vortex on the upper side of the wing. As the laser light was traversed further behind the wing, the vortex remained in good form slightly shifting towards the wing tip in the spanwise position. The tests were performed using a 4 W laser with a pneumatically operated rotating lens. This test is the flow behind the wing which had no fairings placed in the junction.

The oil flow visualizations were carried out for each test case. Figures 9 through 18 show the results of each particular test case. The free stream flow is passing from left to right in the figures. The test with no wing fillets shows the stagnation region ahead of the wing leading edge and the dark lines of the vortex sheet which is rolled up and shed above and below the wing (Ref. 7). A fine dark line with the outer limiting streamline under the wing shows the presence of a secondary or weaker vortical flow which appears to be entrained within the stronger main vortex. At the wing trailing edge, one notices that both vortices follow the flow exiting over the wing trailing edge. As should be expected, there is no indication of separation of the flow at the wing trailing

edge and one sees the wake of the wing clearly defined as it leaves the wing. The test with the fairings in place shows interesting results at both the trailing and leading edge of the wing.

In all cases there is a reduction of the width of the wake at the wing leading edge which manifests itself in a reducing or converging distance between the limiting streamline on the wing upper surface, a shifting of the stagnation point behind the fairing leading edge and wake under the wing which is not as blunt as the wake of the wing without fairings. The faint dark line of secondary flow is also absent in these tests. The trailing edge flow appears to remain unchanged although the wake tends to narrow in size as a result of the fairings. The test with the largest fairing at the trailing edge, figure 10, shows a noticeable improvement in the dimension of the wake.

4.2 Pressure measurements

The five hole probe measured the pressures in the wake of the wing located 1/2 C behind the trailing edge. The probe traversed a plane measuring 60 mm high by 110 mm wide in steps of 5 mm. The flat plate is 5 mm below the traverse plane. The isolines of pressure plots are shown in figures 28 through 36. The values on the ordinate and abscissa represent the percent distance along the two axes. Thus the value .5 would represent 30 mm (50% of 60 mm) in the spanwise direction and 55 mm (50% of 110 mm) along the flat plate trailing edge.

The symbols represent the percentage difference between the value of the point measured and the maximum pressure of the flow. Thus high regions of pressure loss are marked with a diamond symbol.

The isolines of pressure plots indicate the high loss region in the wake of the wing and there are also tunnel flow irregularities which can be seen in all cases. A quick glance

at the plots reveals how the influence of the different fairing combinations is highlighted by studying the isolines of pressure.

The isolines of kinetic energy plots are shown in figures 19 though 27. The plots represent regions of high energy in the wake of the wing which are influenced by the amount of secondary flow entrained into the wake or vortex and hence drag. By examining the kinetic energy footprint of the plots, regions endorsed by the star symbol, the fairings influence is noticeable. The regions of high kinetic energy loss are presented by the half circle symbol and they are indeed located in the center of the wake where the flow is highly stagnant.

The secondary velocity plots proved to provide no information about the size of the vortex. Figure 37 shows that the flow is consistent but certainly erroneous. The downwash of the wing is possibly the overriding factor which aligns the vectors towards the left side of the graph which is the downwash direction. A correction for downwash was made to the data to see if the strong downwash effect could be filtered out. The average value of v, and w was computed over the entire traverse plane and then subtracted from the flow field. The result is somewhat improved but the shedding vortex is still not recognizable with the flow. Figure 37b shows this result.

5. SUMMARY

5.1 Discussion

The crux of the experimental study is the comparison of the vortex size to the pressure and kinetic energy plots, however, since the secondary velocity plots are not sufficiently detailed to visualize and measure the shedding vortex, this comparison is difficult to perform.

Unfortunately, the secondary velocity plots which were corrected for the wing downwash are also not clearly defined to allow a conclusion to be drawn. The plots of pressure and kinetic energy isolines reveal a well defined wake and region of high energy loss, but these plots fail to clearly define a vortex which can be studied and isolated.

The oil flow and the laser sheet flow visualization produced reliable results. The oil flow pictures show a definite change in the surface flow due to the fairing sizes. This effect is very pronounced at the leading edge and not very evident at the trailing edge. A comparison between figures 9 and 10 clearly shows how the leading edge fairing assists the flow to traverse the stagnation zone at the leading edge and continue to pass above and below the wing. The larger leading edge fairings do assist the oncoming flow to pass around the wing leading edge, but they seem to induce a high pressure region located just under the fairing leading edge.

The laser sheet visualization illustrates the shedding vortex as it traverses the wing growing in size and shifting in the spanwise direction away from the wing junction. The vortex is well defined and shows good agreement with previous work by Shabaka on wing body junctions (Ref. 4).

5.2 Conclusions

The absence of the secondary velocity plots make a conclusion difficult to be drawn. The isolines of kinetic energy indicate that the leading edge fairings of the smallest size yield a small kinetic energy footprint. Most important are the oil flow visualization pictures which clearly indicate that the small leading edge fairing permits the flow to pass smoothly along the wing. Therefore, it can be said that the small leading edge fairing, based on flow visualization and isolines of kinetic plots, produced the best flow qualities. The oil flow tests also indicate that the large fairing chords C_f are not as effective in reducing the wake at the wing leading edge as the smallest fairing chord is. A study of the kinetic energy plots indicated that the small leading edge fairing induced less flow into the shedding vortex than the large fairings and therefore it can be said that the small fairing was more effective. This conclusion is based on both the oil flow and pressure tests. The effect of the trailing edge fairing appears to be small at best.

5.3 Recommendations

Due to the fact that the probe did not produce plots of well defined vortices behind the wing, two reasons could be inferred. The first possibility is that the flow angularities were small. The probe, which was calibrated at a roll angle of 20°, did exhibit non linear behaviour at small angles of attack. Perhaps if the probe was to be calibrated for smaller roll angles the problem could be unmasked or fixed.

The second possibility is that the strength of the vortex is indeed weak compared to the downwash at the wing trailing edge. Thus the downwash vector v might have a large order of magnitude compared to the velocity vector w, which would influence the resultant angle between the two vectors. This resultant angle between the velocity vectors v and w gives

the shape of the vortex which is plotted by the computer program.

An interesting experiment in the flow visualization area might be to test the wing and fairings in a water tunnel or a water table to observe the three dimensional flow in the junction.

REFERENCES

1. JACOBS, E.N. & WARD, K.: *Interference of wing and fuselage* from tests of 209 combinations in the NACA variable density tunnel.
NACA R 540, 1935.

2. KÜCHEMANN, D. The aerodynamic design of aircraft.
Oxford, Pergamon Press, 1978.

3. JUPP, J.A.: Interference aspects of the A310 high speed wing configuration. In:
"Subconic/Transonic Configuration Aerodynamics",
AGARD CP 285, 1980, paper 11.

4. SHABAKA, I.M.M.A. & BRADSHAW, P.: Turbulent flow measurements in an idealized wing/body junction.
AIAA J., Vol 19, No. 2, Feb. 1981, pp 131-132.

5. WICKENS, R.; SOUTH, P.; RANGI, R.S.; HENSHAW, D.: Experimental developments in V/STOL wind tunnel testing at the National Aeronautical Establishement.
Canadian Aeronautics & Space Journal, Vol. 19, No. 4, April 1974, pp 145-154.

6. JEUSETTE, J.: Etude du sillage du capotage du train d'atterrissage d'un avion cargo.
U-VKI 1983-10.

7. SCHMITZ, F.W.: Aerodynamik des Flugmodells Tragflügelmessungen 1.
C.J.E. Volkmann Nachf E. Wette, Berlin, 1942.

WING

type : straight, untwisted

profile : NACA 0010

chord : 180 mm

span : 180 mm

Re_c : $.28 \times 10^6$

WIND TUNNEL

type : VKI L-2A low speed suction tunnel

dimensions : : 300 mm Ø test section

testing velocity : 50 mm H_2O, 28.3 m/s

TABLE 1 - MODEL GEOMETRY AND WIND TUNNEL SPECIFICATIONS

TEST		FAIRING SIZE L.E.	T.E.
1		no fairings	
2		.1 C,	.3 C
3		.1 C,	.2 C
4		.1 C,	.1 C
5		.2 C,	.3 C
6		.2 C,	.2 C
7		.2 C,	.1 C
8	(acquisition failure)	.3 C,	.3 C
9		.3 C,	.2 C
10		.3 C	.1 C

TABLE 2 - SUMMARY OF TESTS

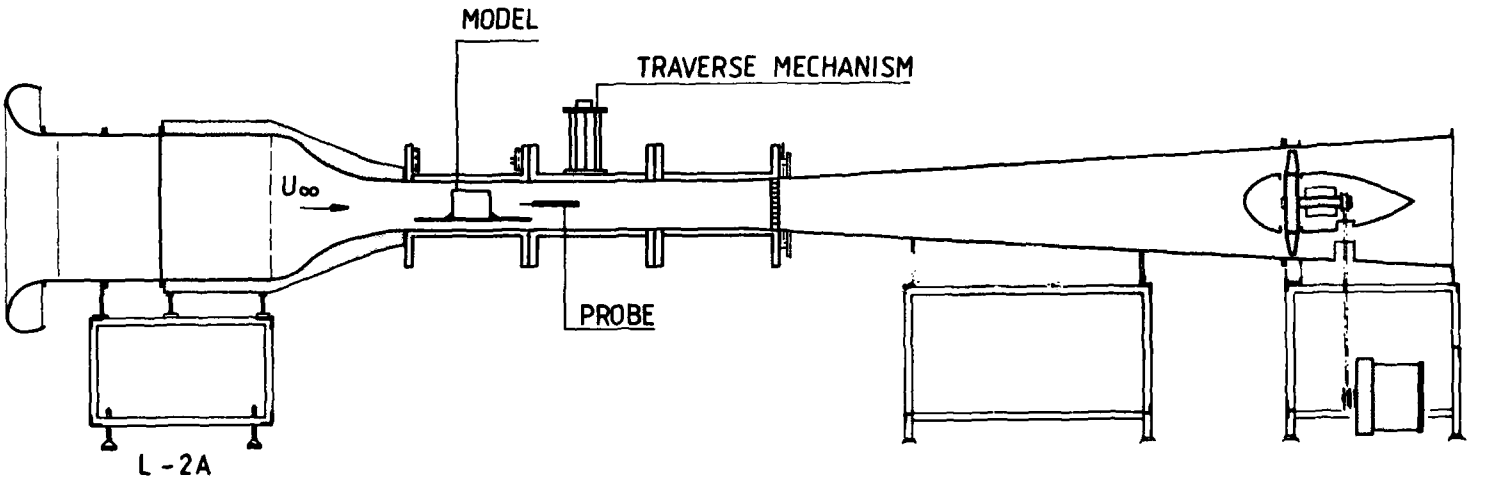

FIG. 1 - VIEW OF WIND TUNNEL AND TEST MODEL

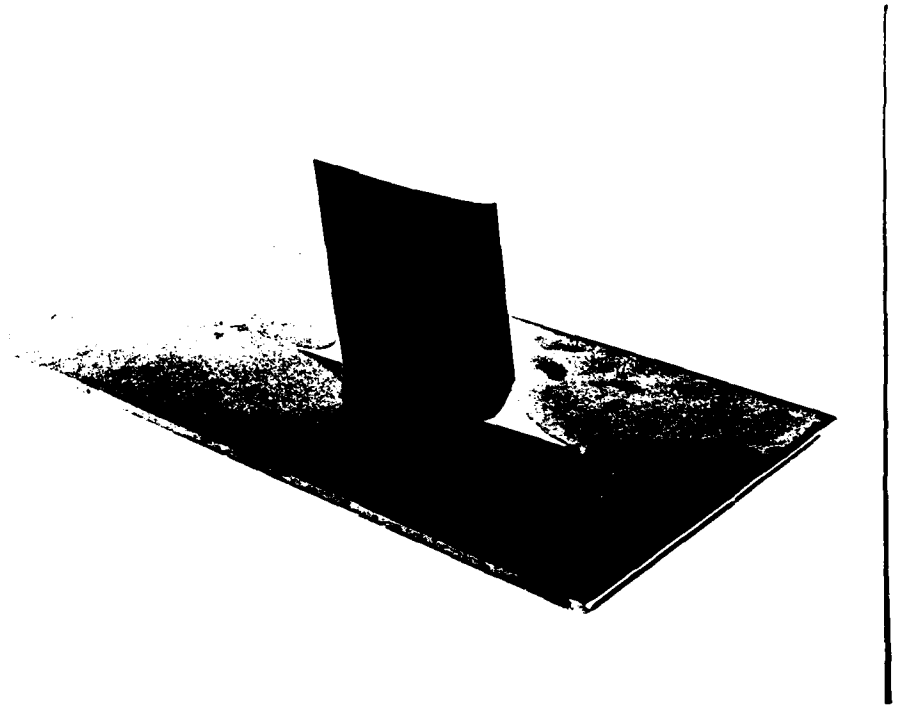

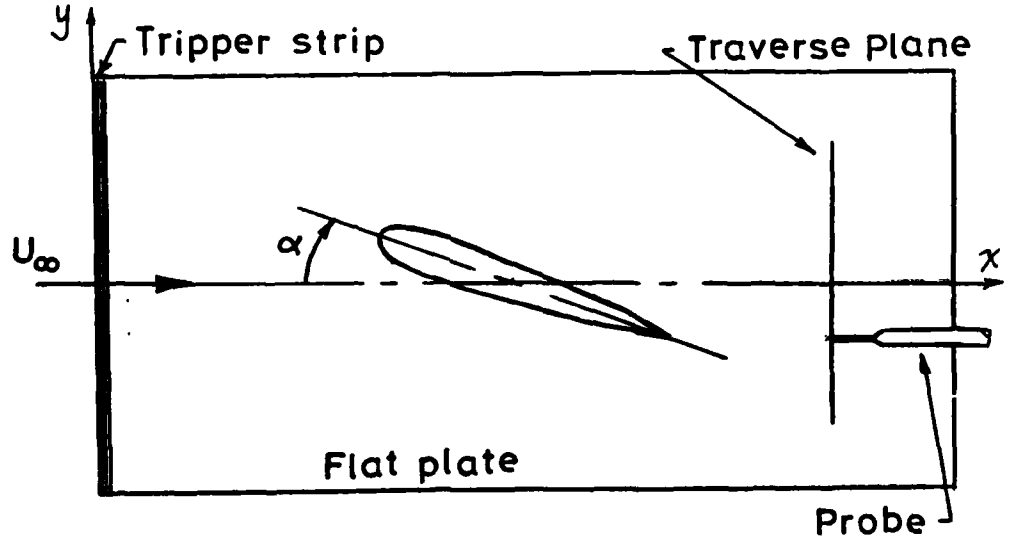

FIG. 2 - TEST MODEL

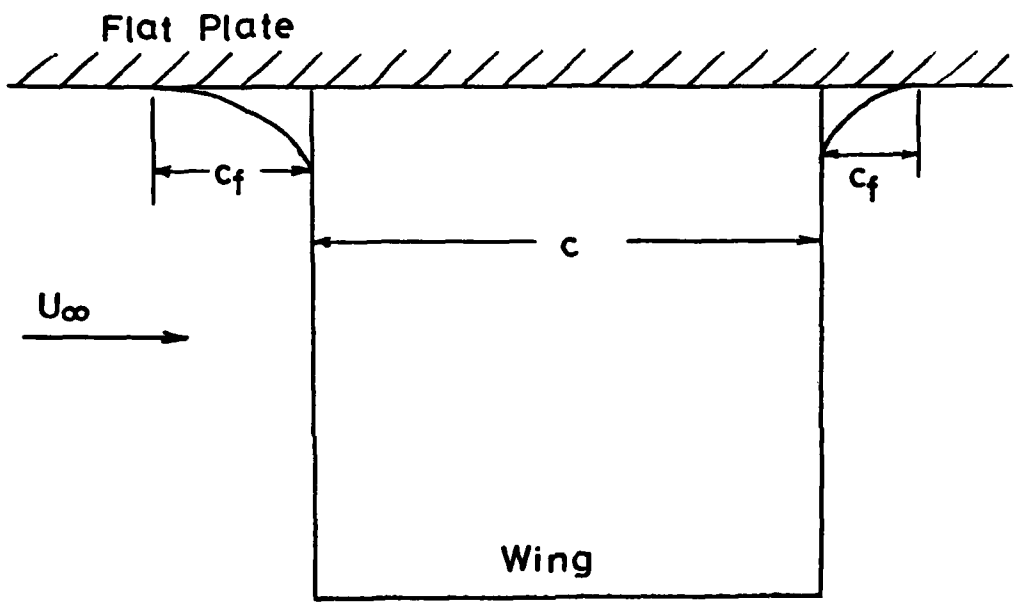

C = 180 mm

C_f = .1 C, .2 C, .3 C

Fairings = elliptical family of curves C = .860

FIG. 3 - FAIRING GEOMETRY

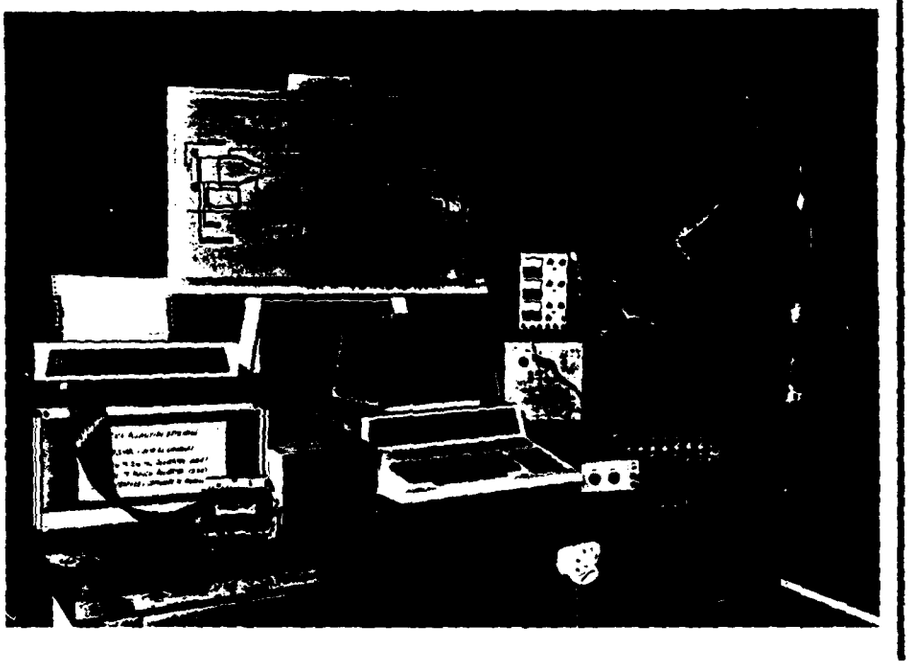

FIG. 4 - THE EXPERIMENTAL SET-UP

FIG. 5 - FIVE HOLE PRESSURE PROBE

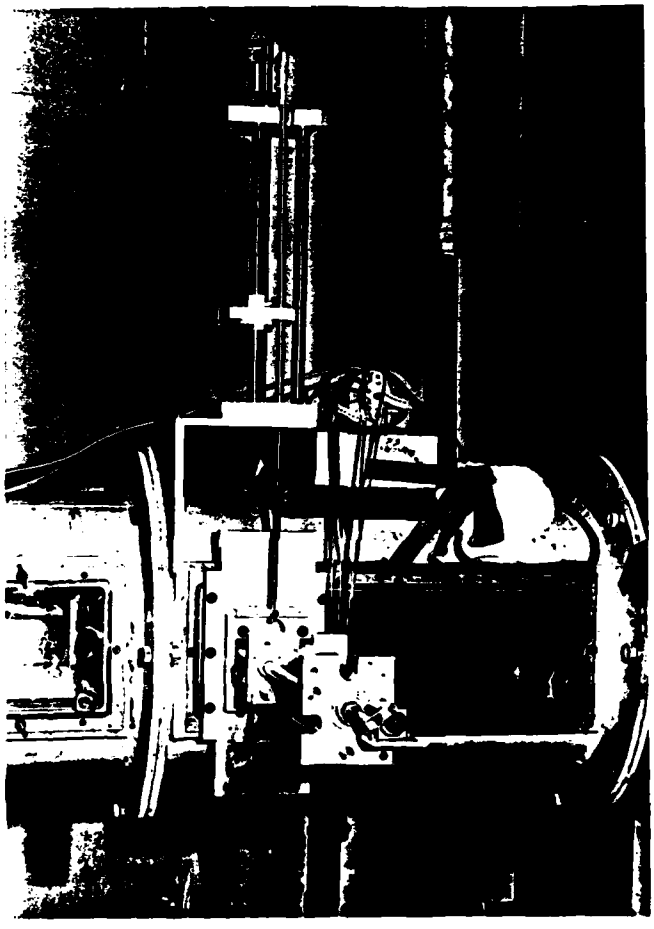

FIG. 6 - TRAVERSE MECHANISM

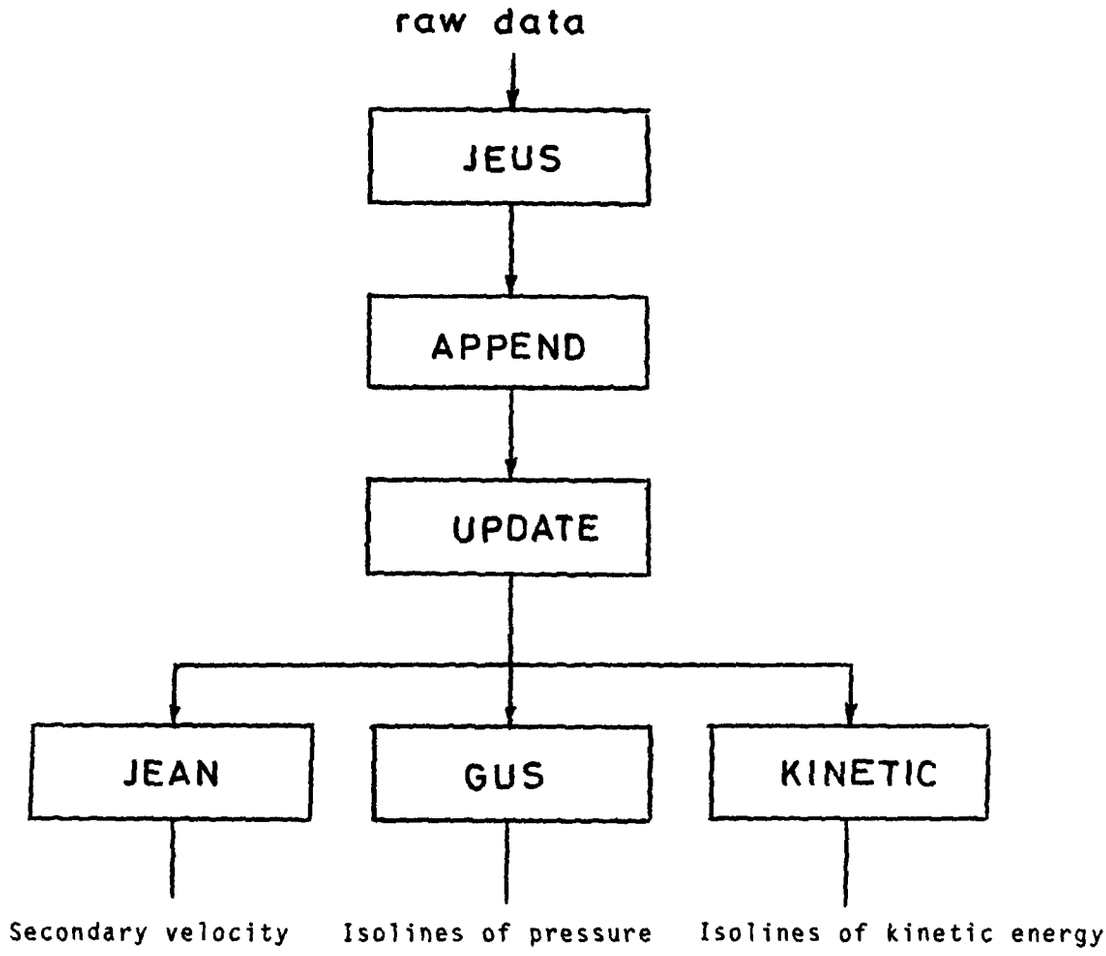

FIG. 7 - DATA REDUCTION FLOW CHART

(a) At wing trailing edge

(b) 1/2 C behind wing trailing edge

(c) 1 1/2 C behind wing trailing edge

FIG. 8 - LASER LIGHT FLOW VISUALIZATION

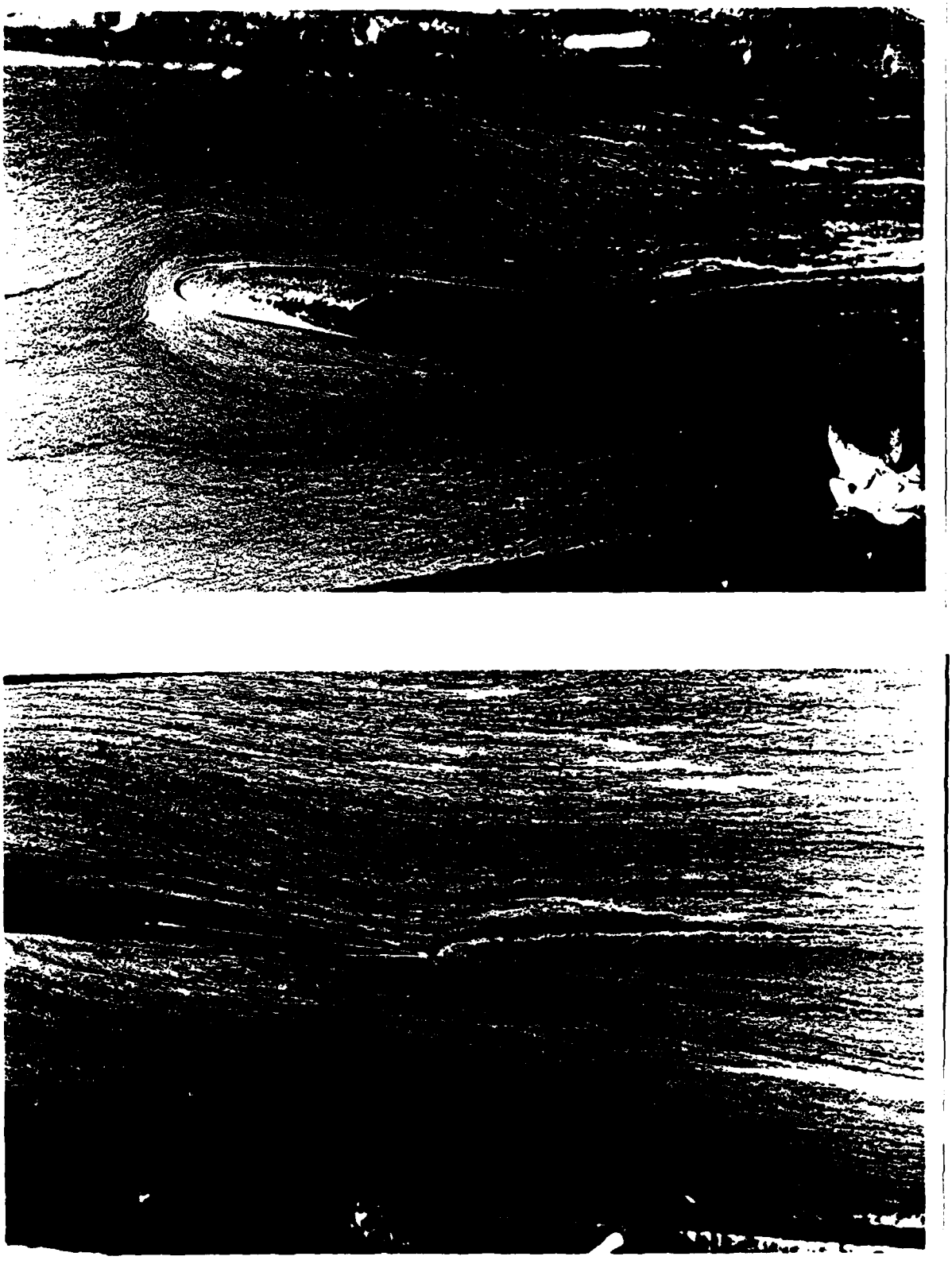

FIG. 9 - WING WITHOUT FAIRINGS

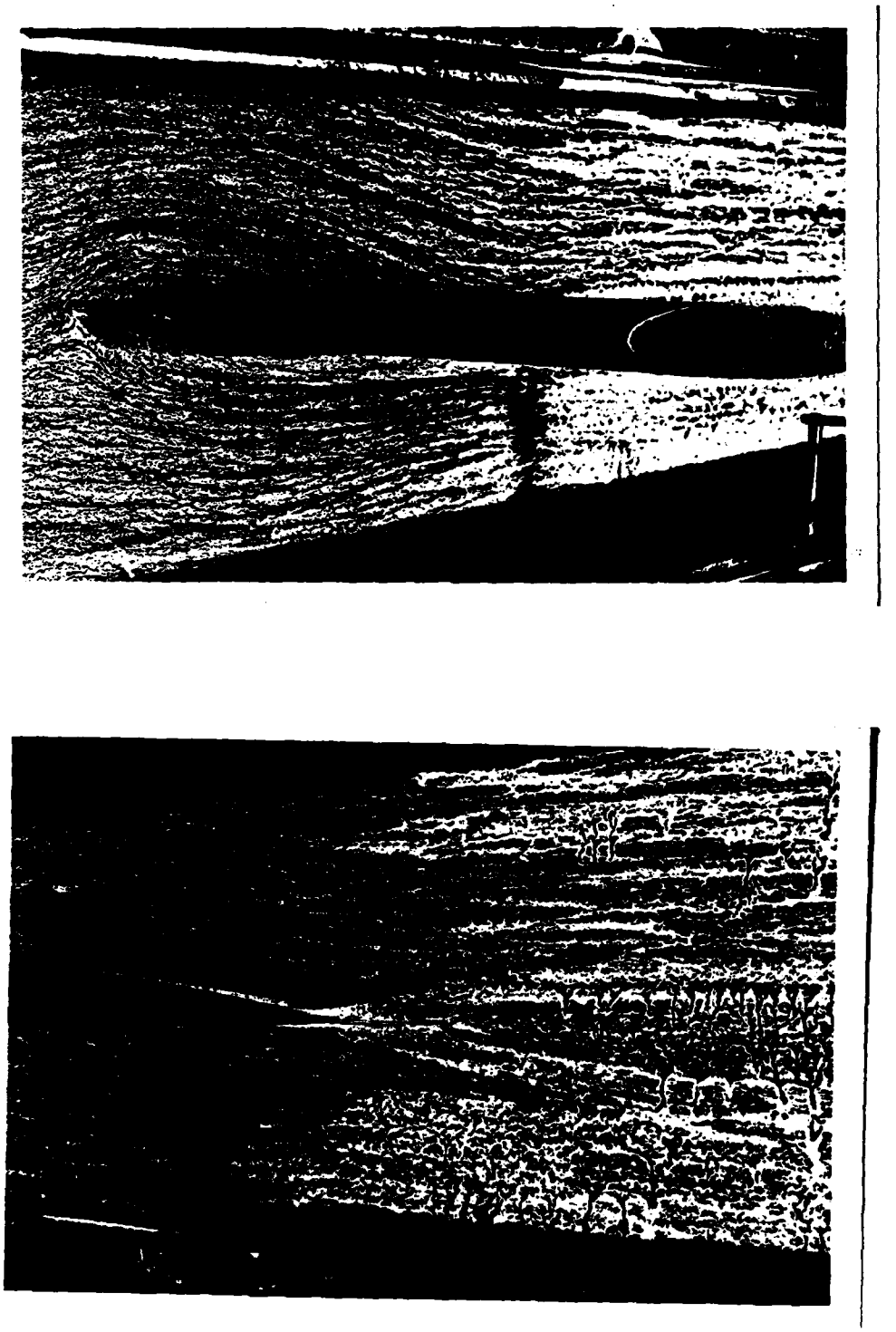

FIG. 10 - OIL FLOW VISUALIZATION - TEST 2

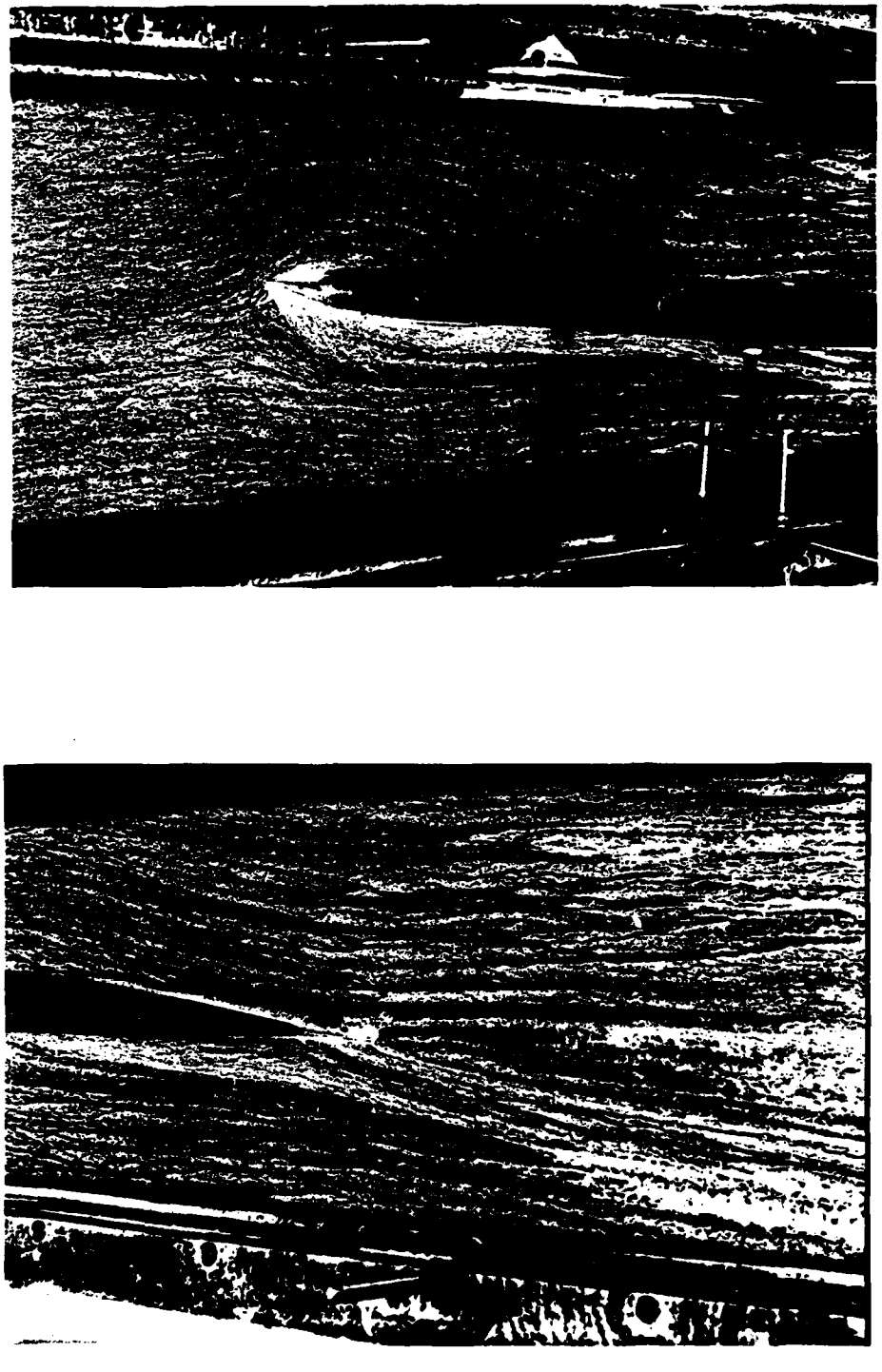

FIG. 11 - OIL FLOW VISUALIZATION - TEST 3

FIG. 12 - OIL FLOW VISUALIZATION - TEST 4

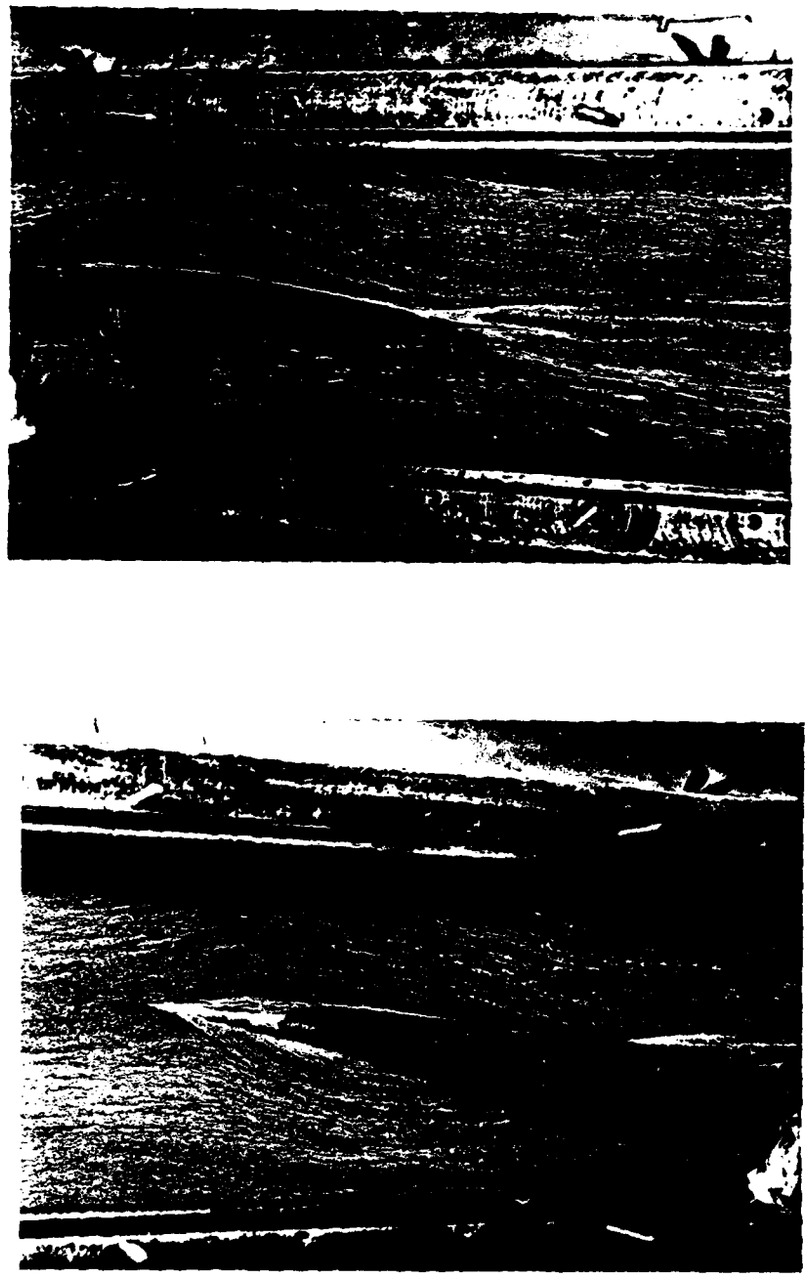

FIG. 13 - OIL FLOW VISUALIZATION - TEST 5

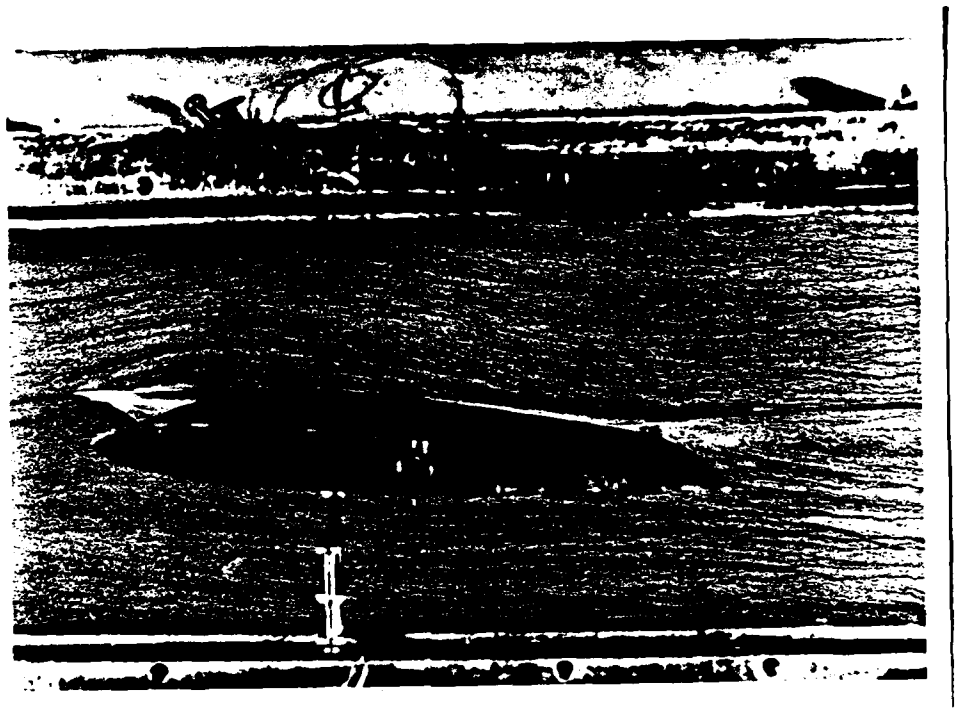

FIG. 14 - OIL FLOW VISUALIZATION - TEST 6

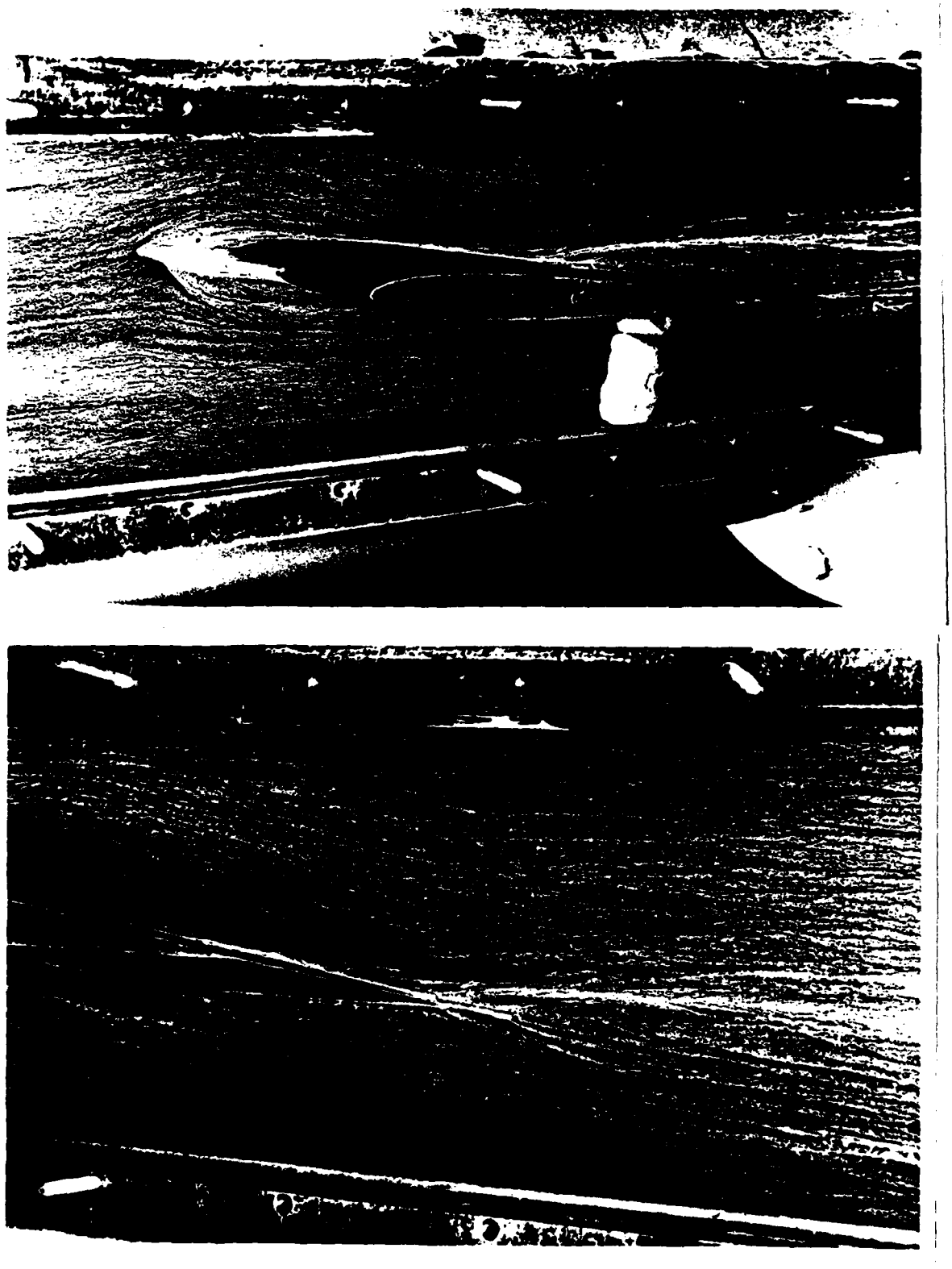

FIG. 15 - OIL FLOW VISUALIZATION - TEST 7

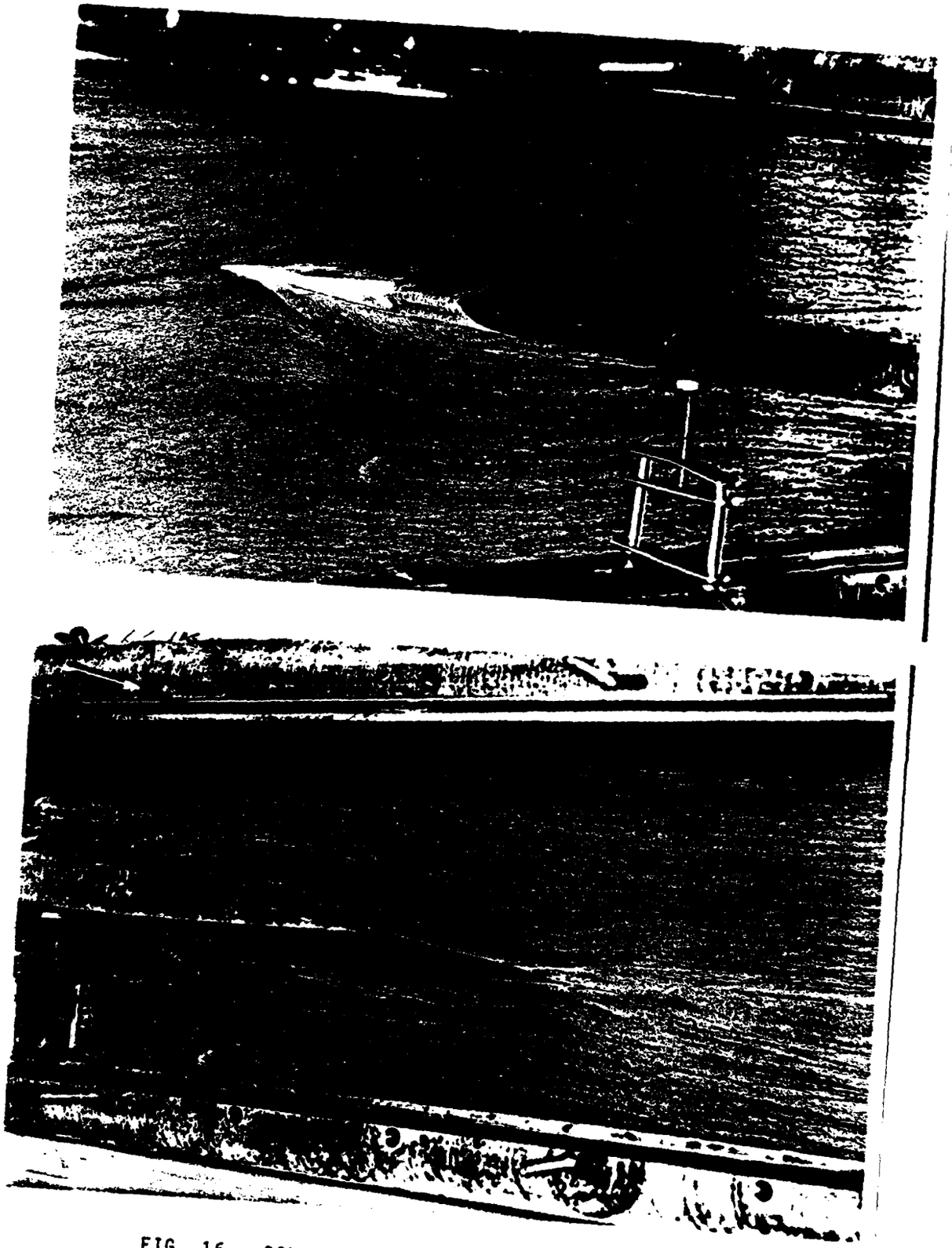

FIG. 16 - OIL FLOW VISUALIZATION - TEST 8

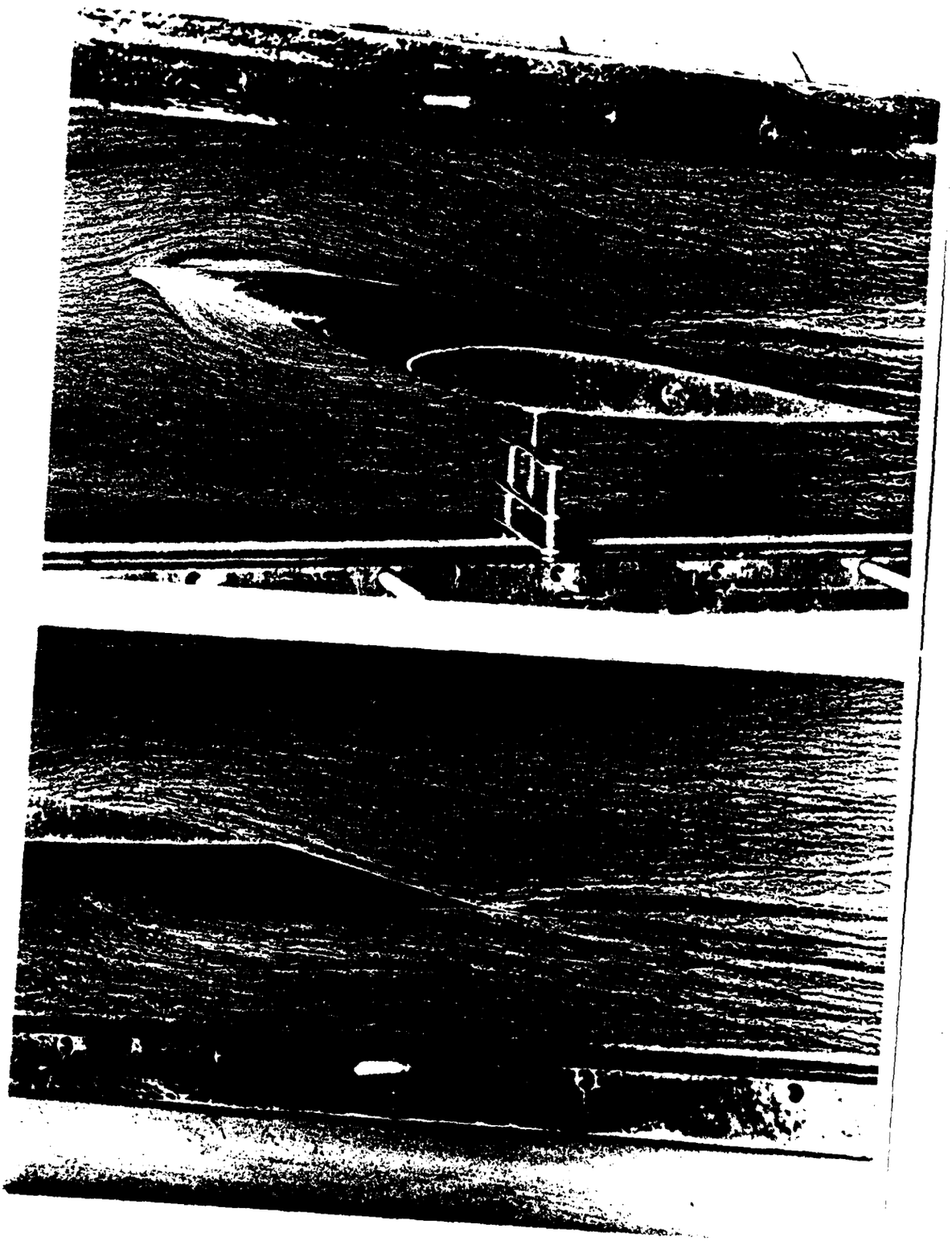

FIG. 17 - OIL FLOW VISUALIZATION - TEST 9

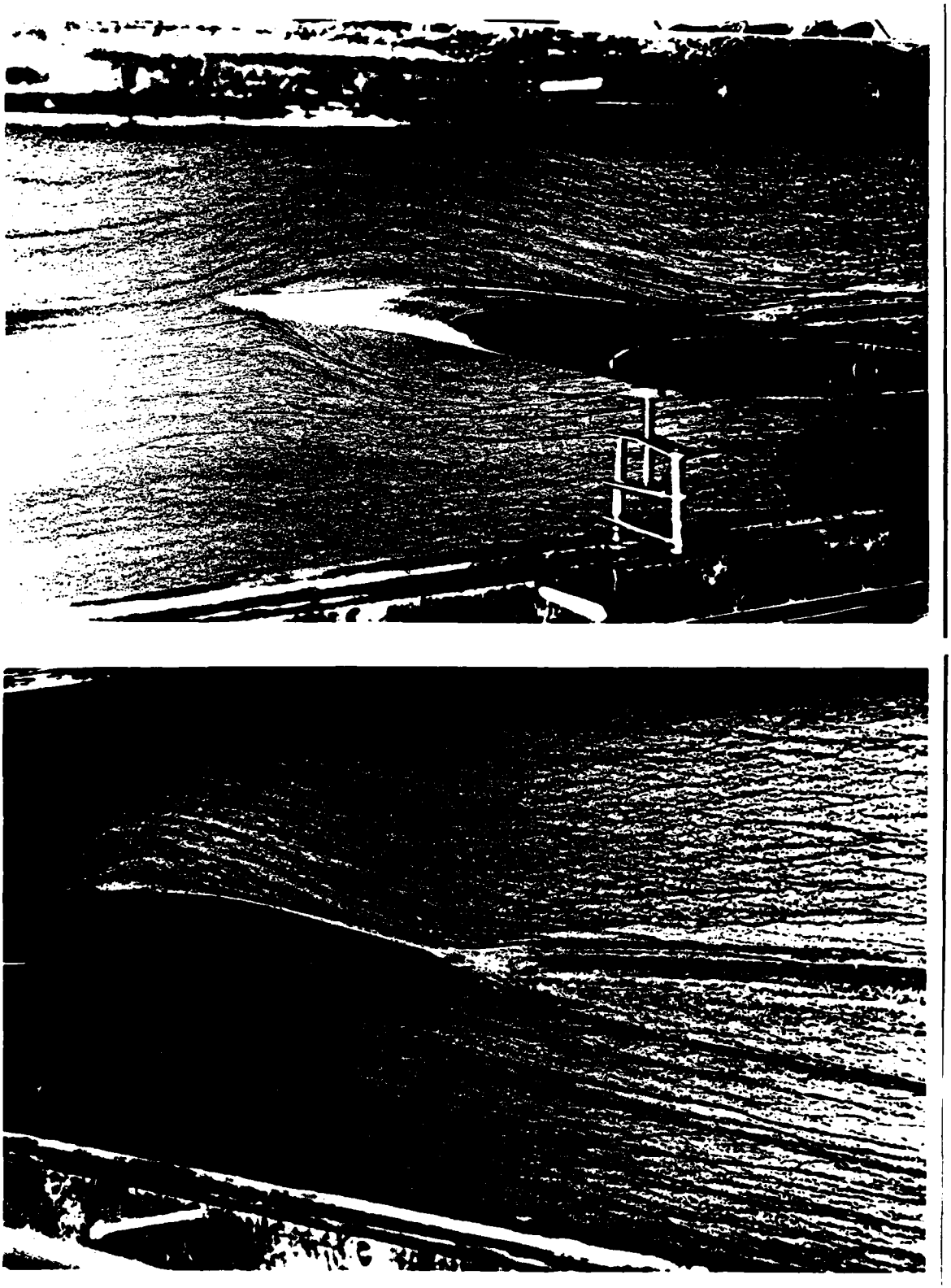

FIG. 18 - OIL FLOW VISUALIZATION - TEST 10

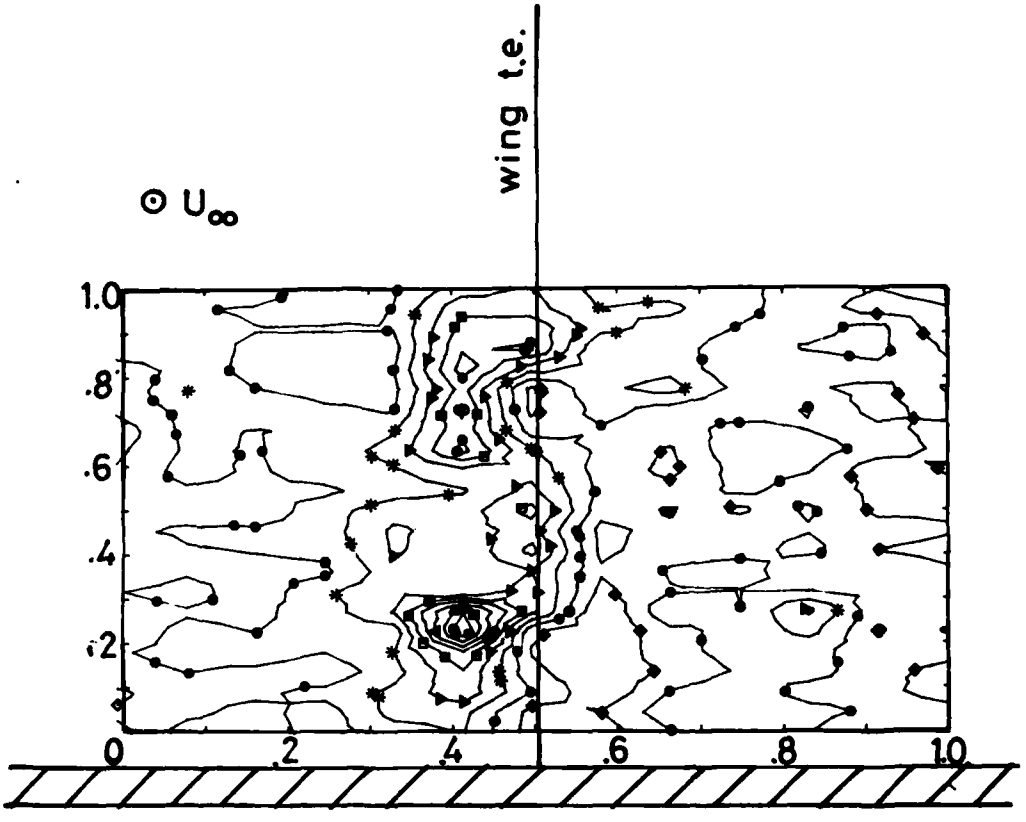

Flat plate

Traverse plane dimensions
60 mm × 110 mm

Velocity = 28 m/s

◇	0.10
○	0.20
✳	0.30
▲	0.40
▪	0.50
●	0.60
▼	0.70
■	0.80
⊖	0.90

FIG. 19 - ISOLINES OF KINETIC ENERGY - TEST 1

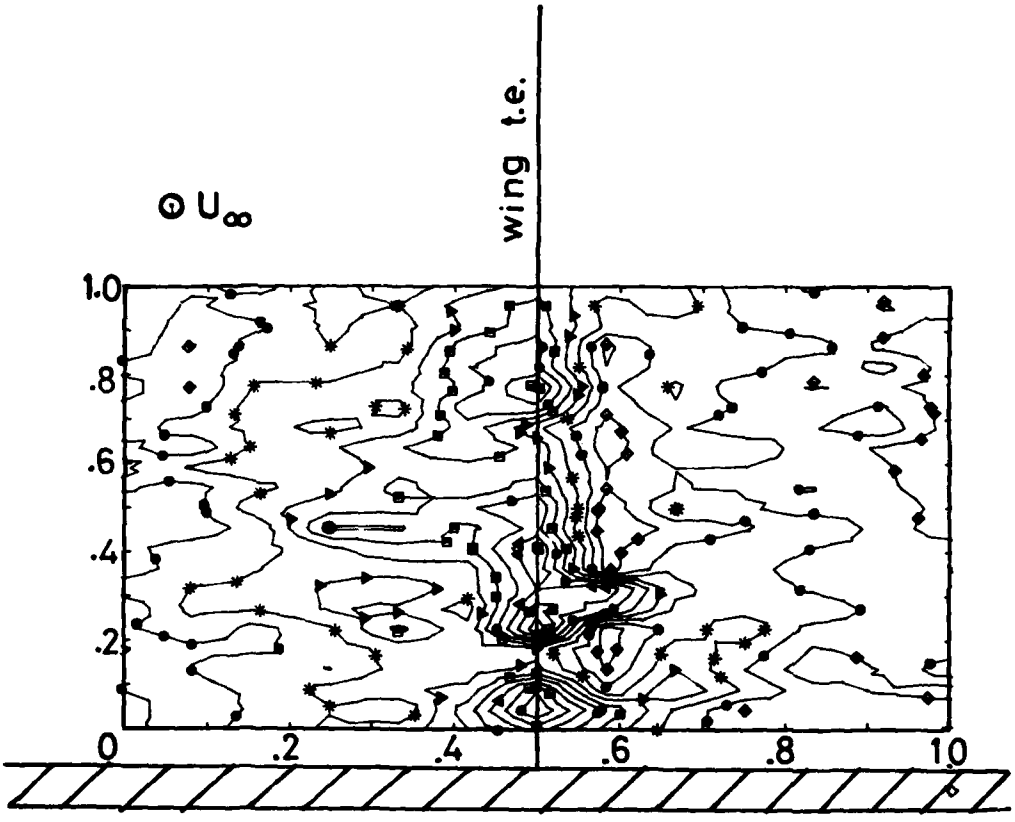

Flat plate

Traverse plane dimensions
60 mm × 110 mm

Velocity = 28 m/s

FIG. 20 - ISOLINES OF KINETIC ENERGY - TEST 2

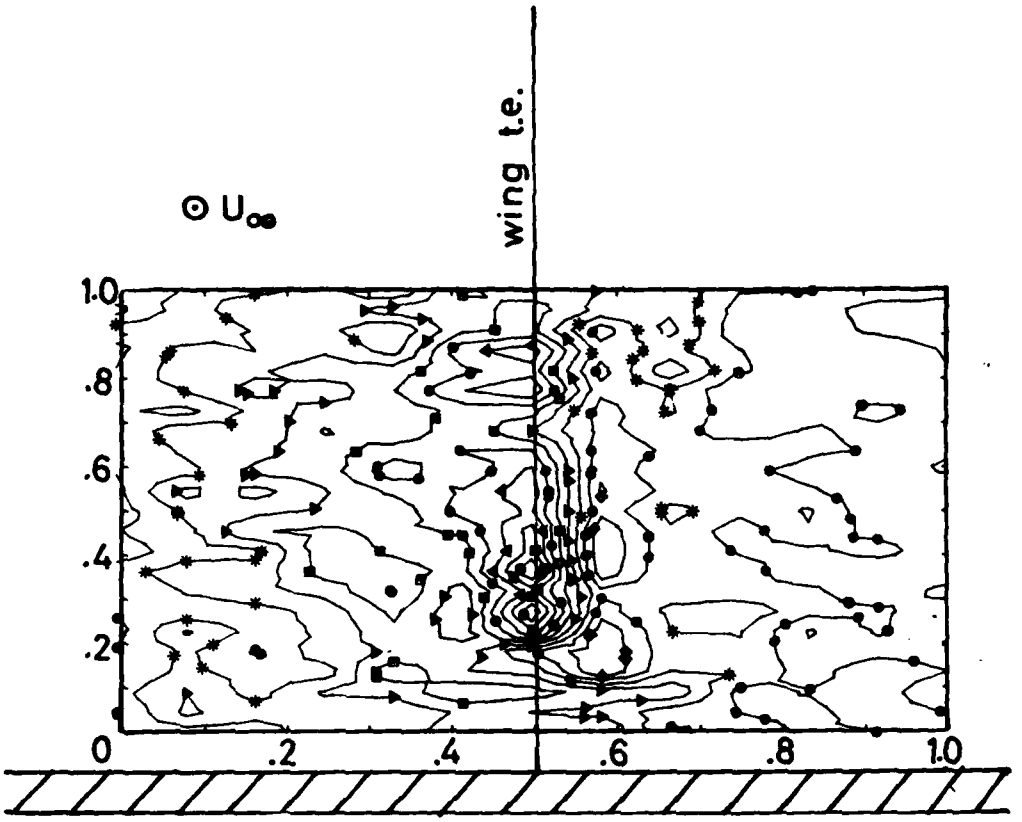

Flat plate

Traverse plane dimensions
60 mm × 110 mm

Velocity = 28 m/s

FIG. 21 - ISOLINES OF KINETIC ENERGY - TEST 3

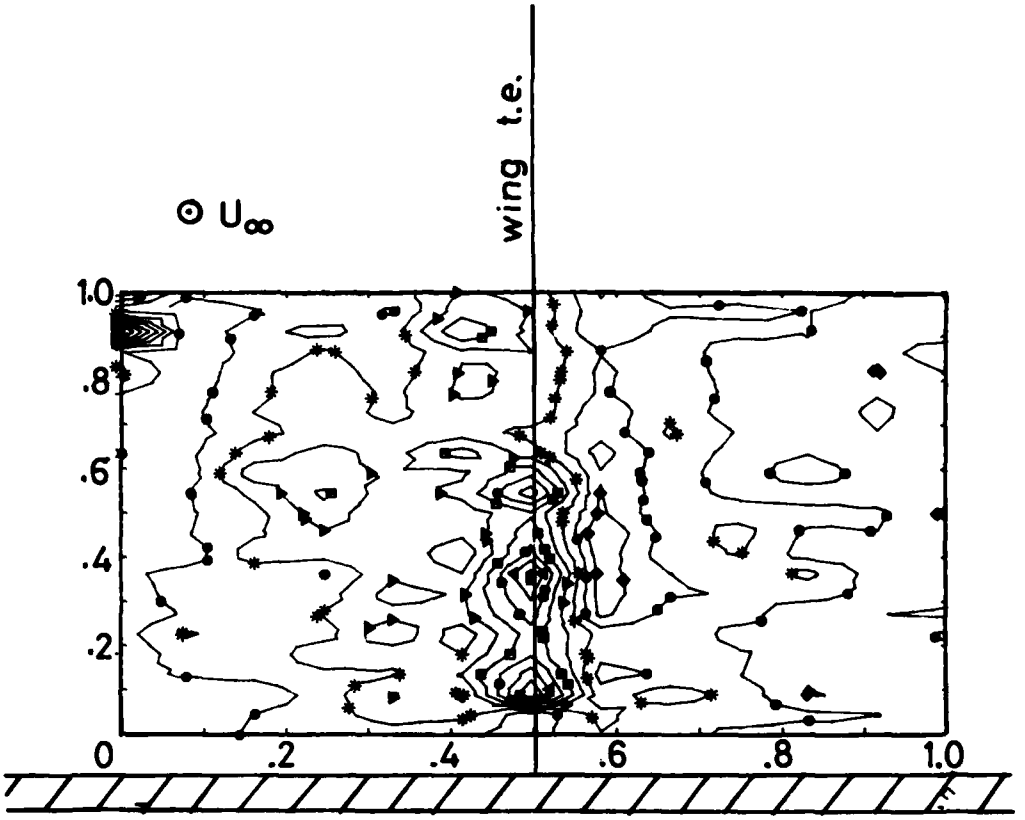

Flat plate

Traverse plane dimensions
60 mm × 110 mm

Velocity = 28 m/s

FIG. 22- ISOLINES OF KINETIC ENERGY - TEST 4

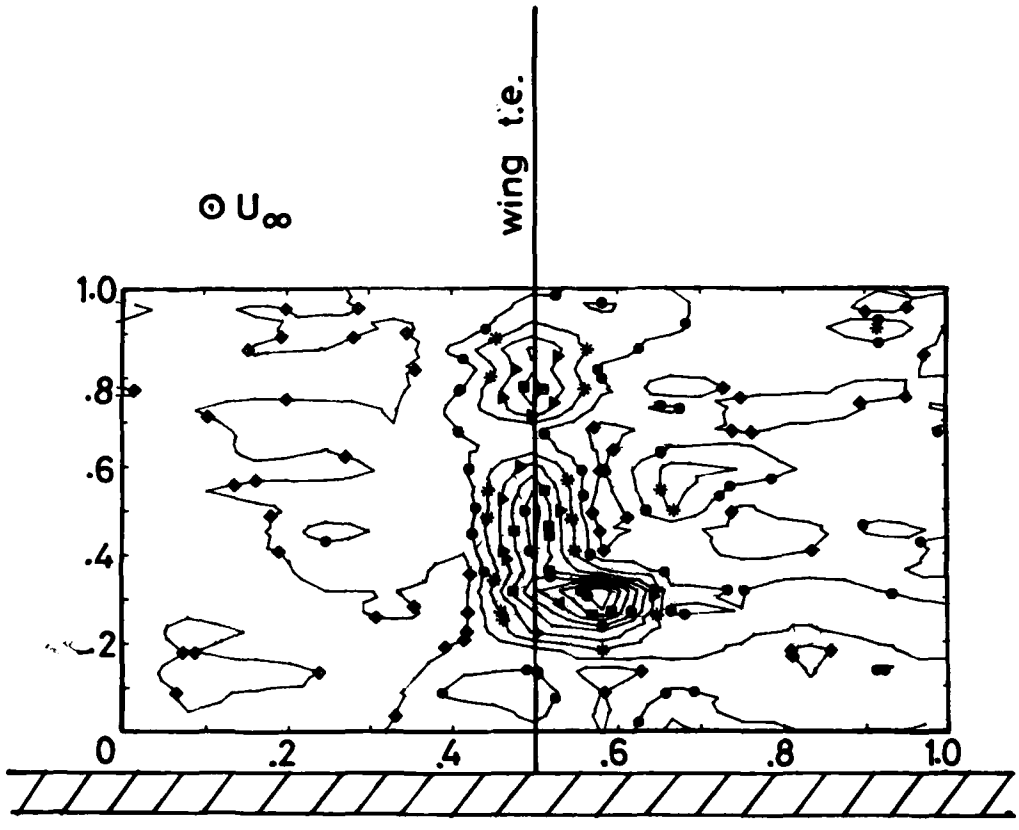

Flat plate

Traverse plane dimensions
60 mm × 110 mm

Velocity = 28 m/s

FIG. 23 - ISOLINES OF KINETIC ENERGY - TEST 5

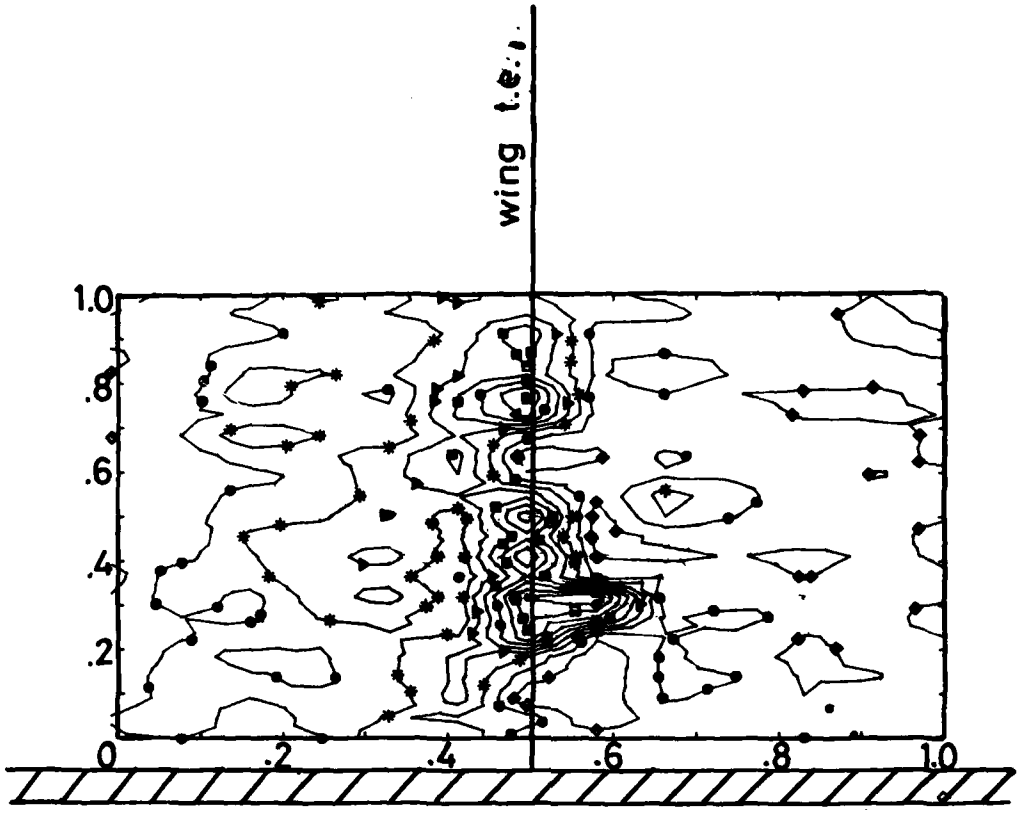

Flat plate

Traverse plane dimensions
60 mm × 110 mm

Velocity = 28 m/s

FIG. 24 - ISOLINES OF KINETIC ENERGY - TEST 6

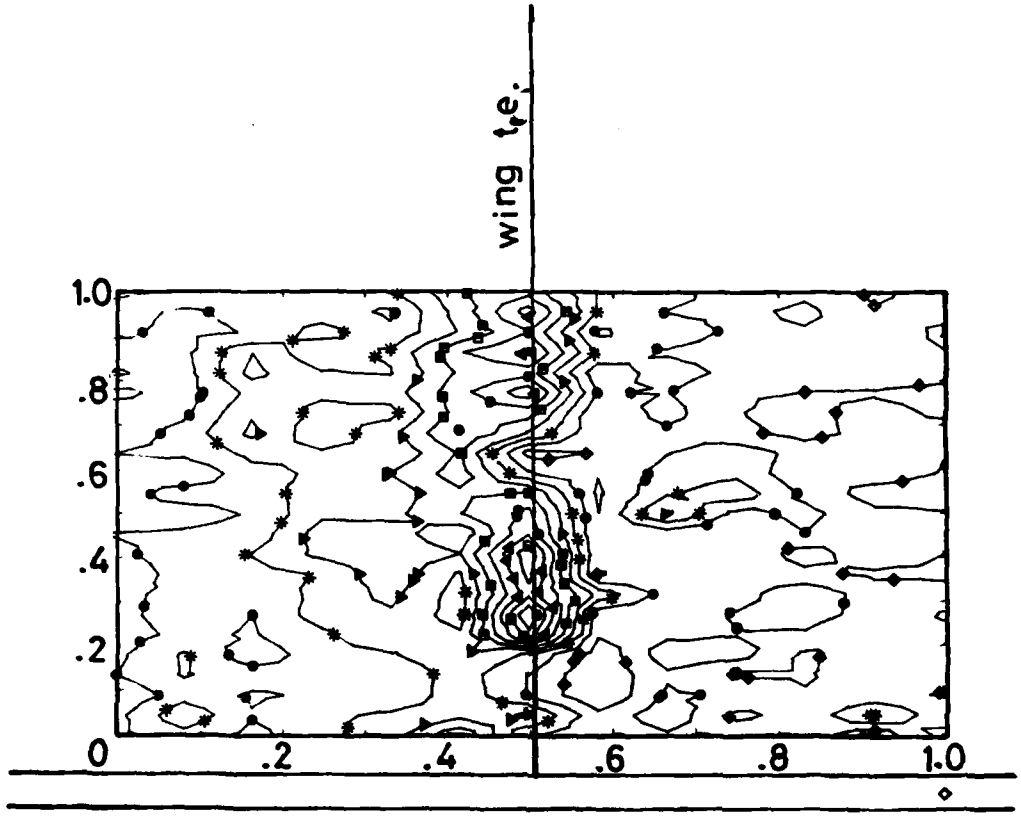

Flat plate

Traverse plane dimensions
60 mm × 110 mm

Velocity = 28 m/s

FIG. 25 - ISOLINES OF KINETIC ENERGY - TEST 7

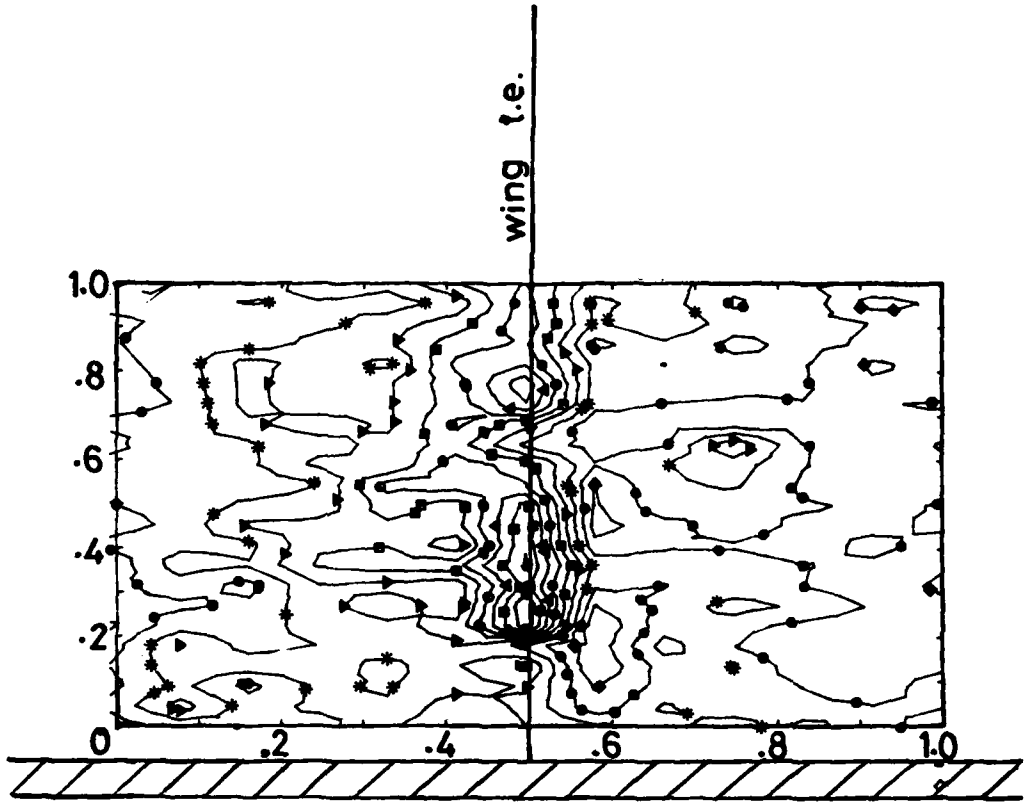

Flat plate

Traverse plane dimensions
60 mm × 110 mm

Velocity = 28 m/s

FIG. 26 - ISOLINES OF KINETIC ENERGY - TEST 9

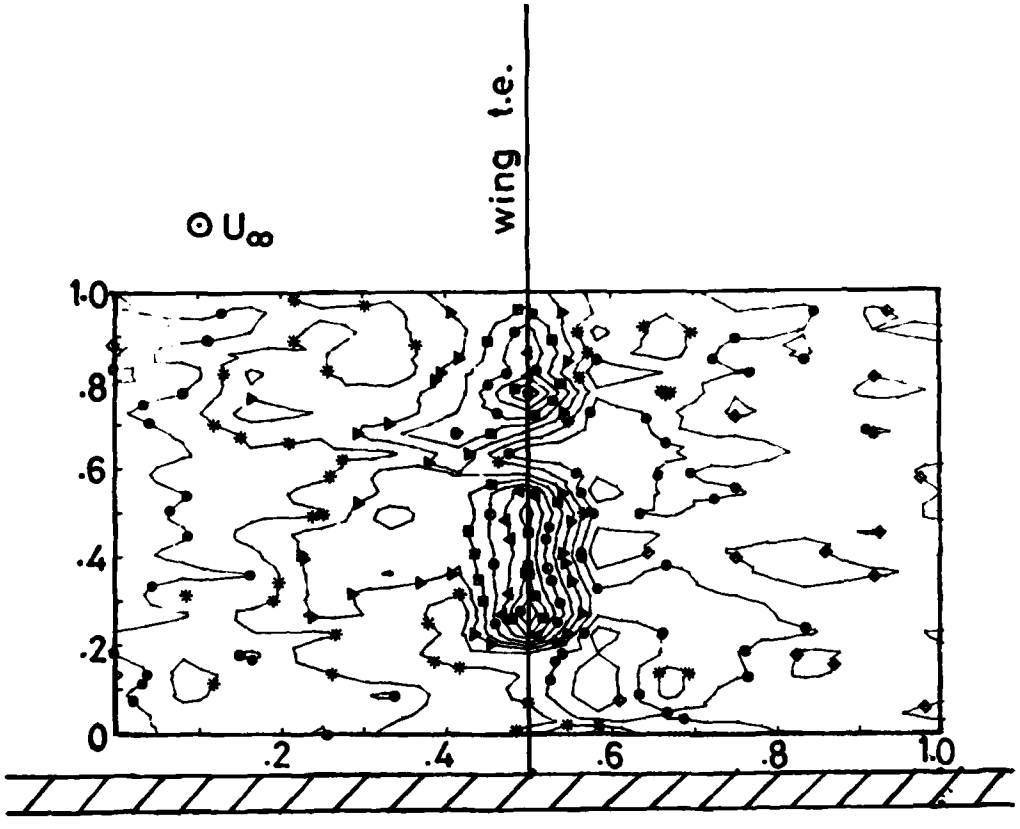

Flat plate

Traverse plane dimensions
60 mm × 110 mm

Velocity = 28 m/s

FIG. 27 - ISOLINES OF KINETIC ENERGY - TEST 10

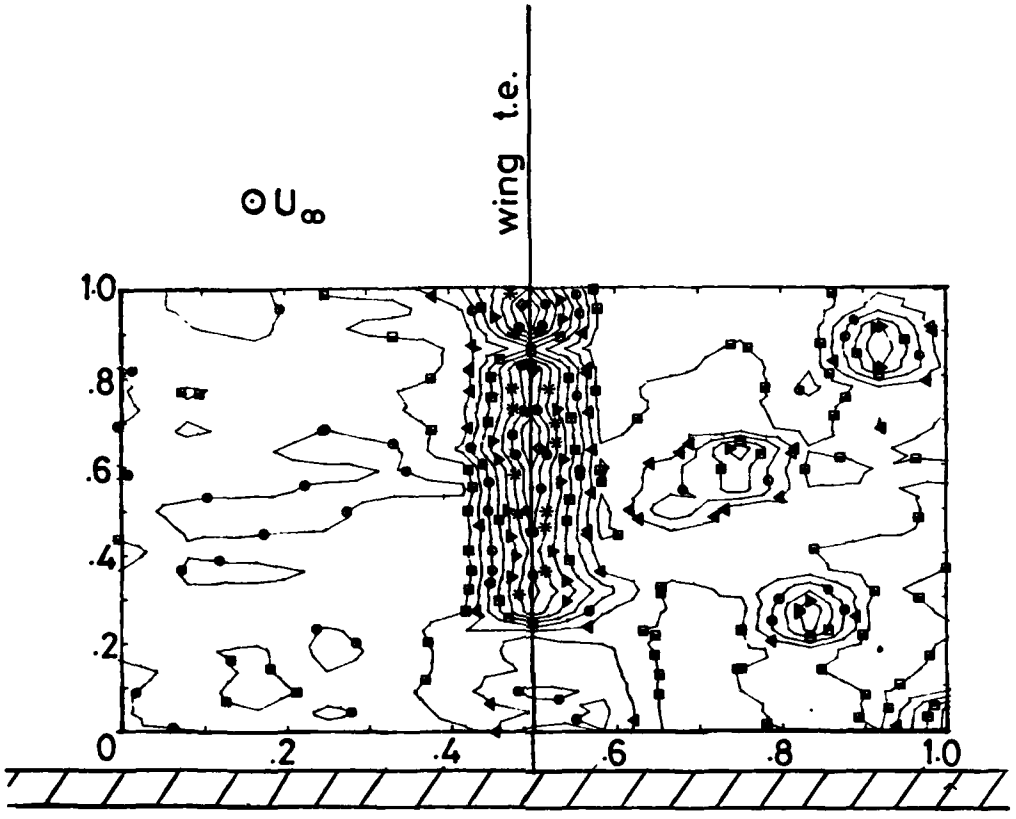

Flat plate

Traverse plane dimensions
60 mm × 110 mm

Velocity = 28 m/s

FIG. 28 - ISOLINES OF PRESSURE - TEST 1

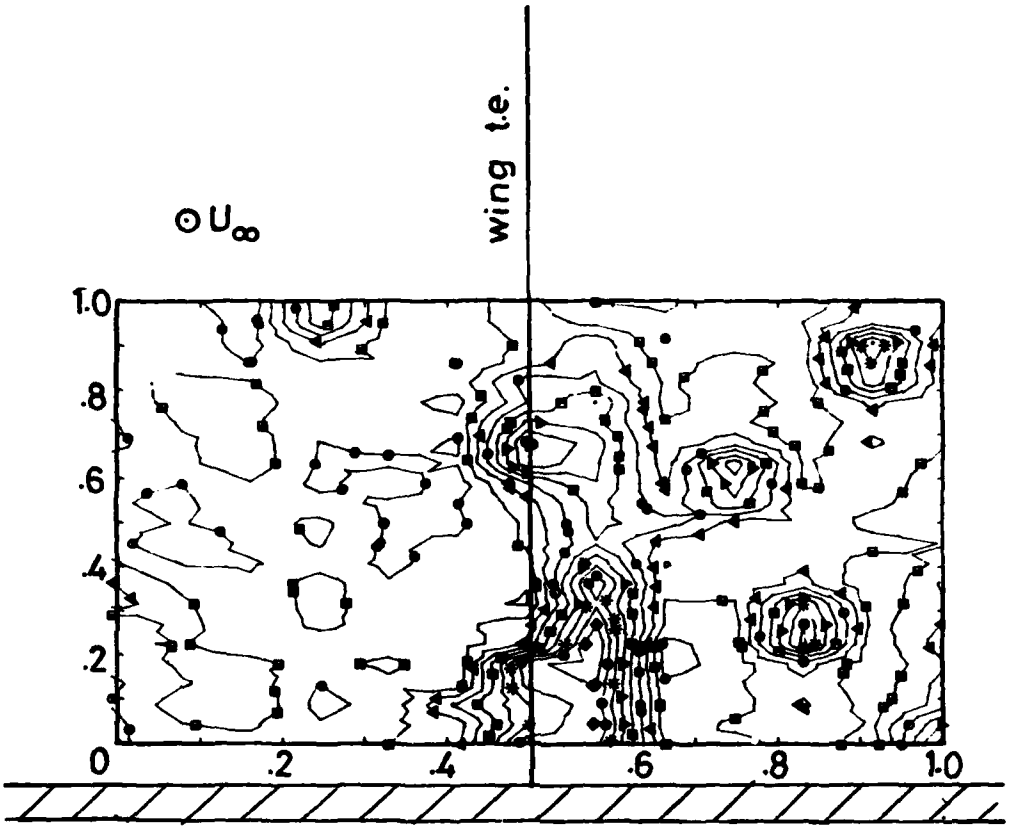

Flat plate

Traverse plane dimensions
60 mm × 110 mm

Velocity = 28 m/s

FIG. 29 - ISOLINES OF PRESSURE - TEST 2

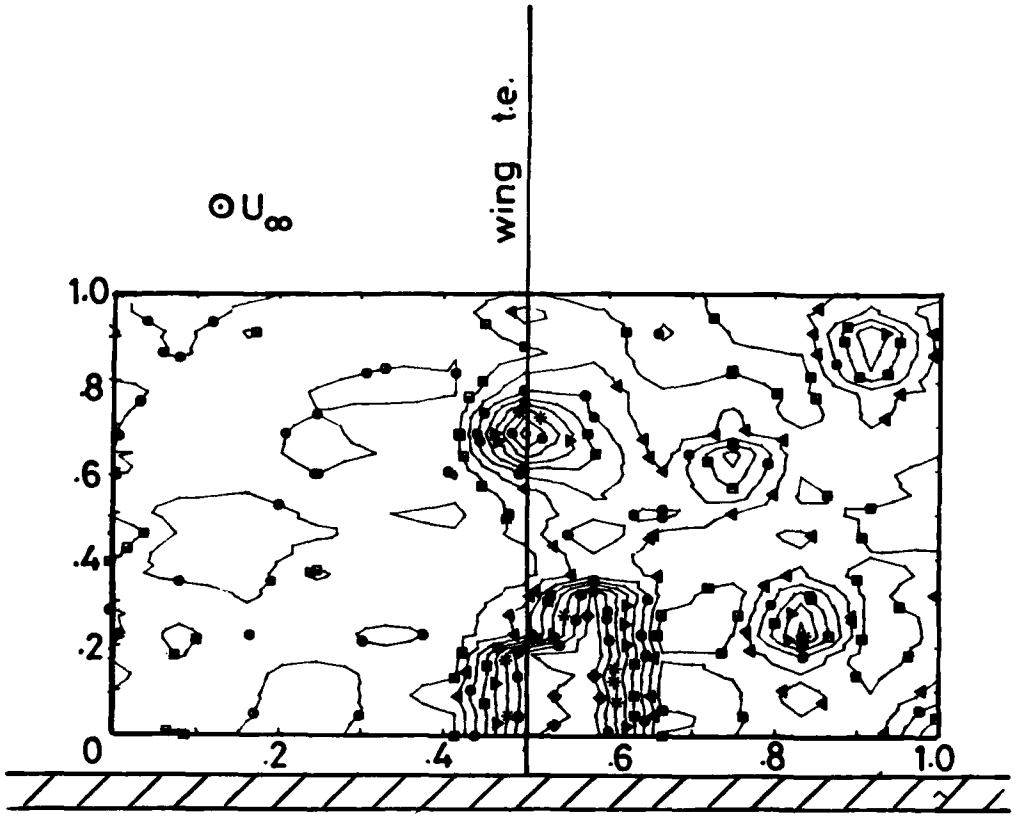

Flat plate

Traverse plane dimensions
60 mm × 110 mm

Velocity = 28 m/s

FIG. 30 - ISOLINES OF PRESSURE - TEST 3

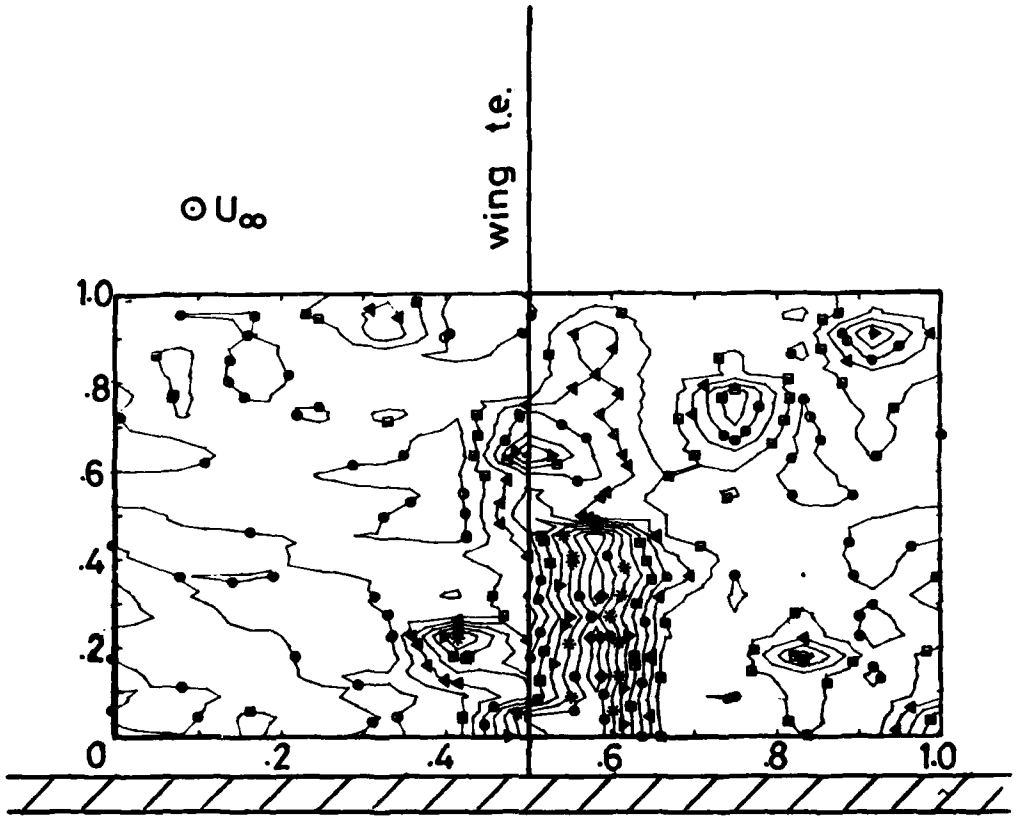

Flat plate

Traverse plane dimensions
60 mm × 110 mm

Velocity = 28 m/s

FIG. 31 - ISOLINES OF PRESSURE - TEST 4

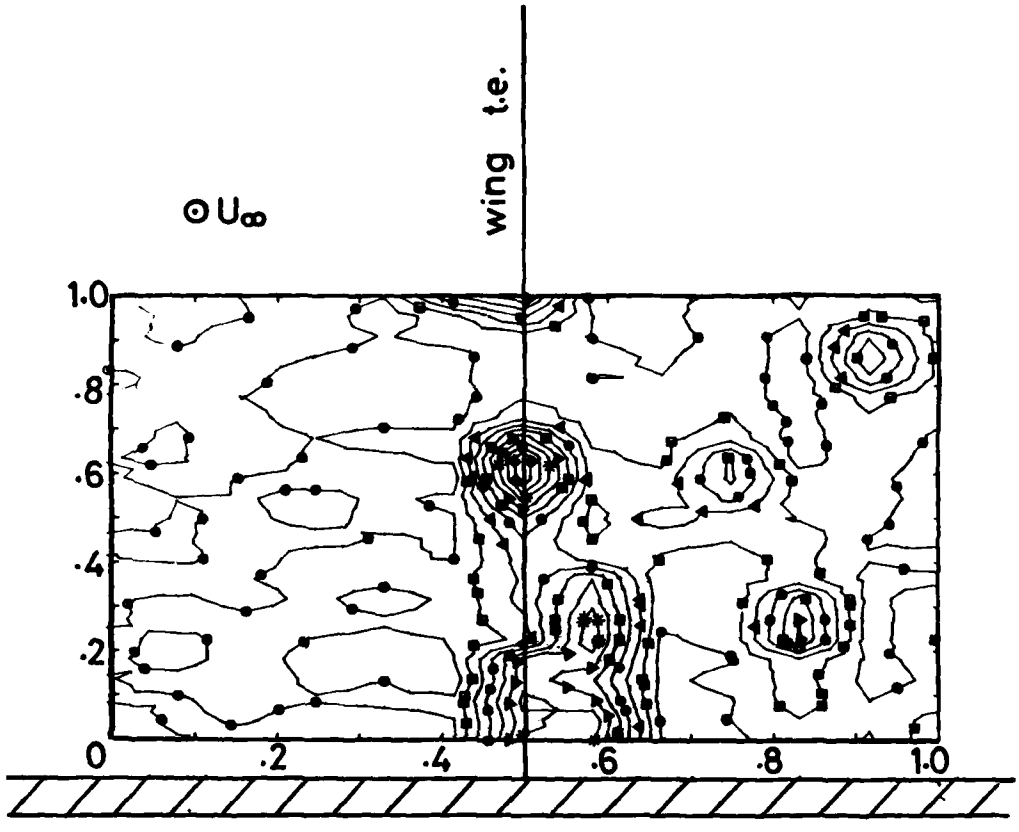

Flat plate

Traverse plane dimensions
60 mm × 110 mm

Velocity = 28 m/s

FIG. 32 - ISOLINES OF PRESSURE - TEST 5

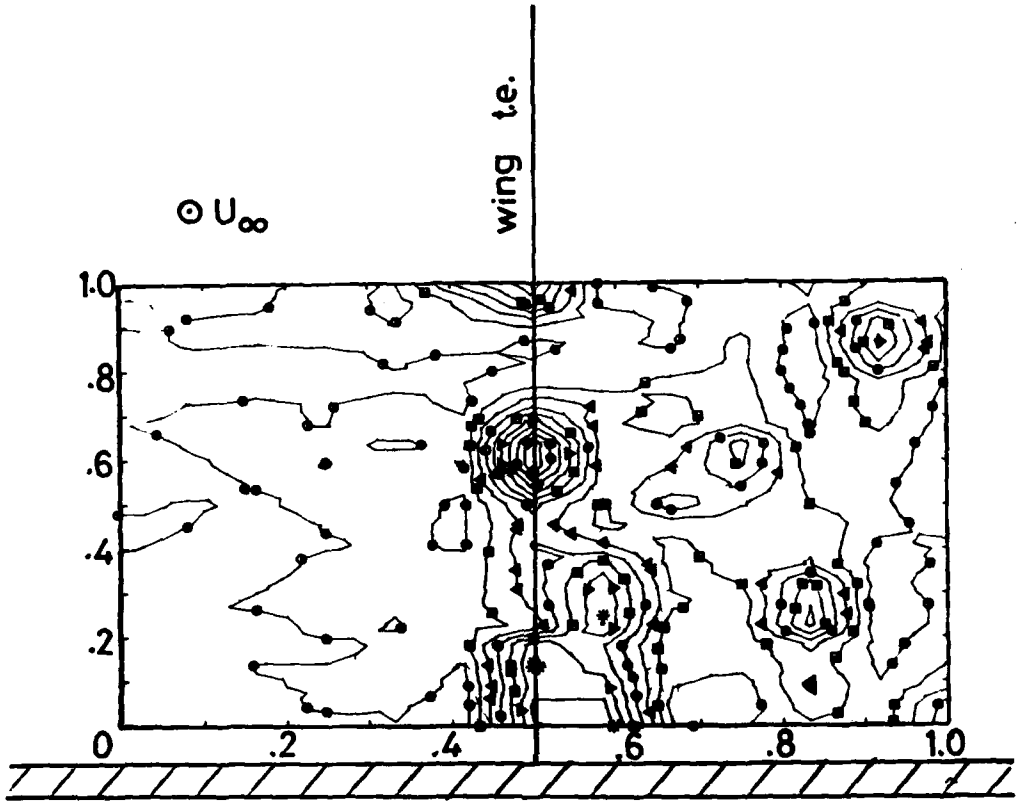

Flat plate

Traverse plane dimensions
60 mm × 110 mm

Velocity = 28 m/s

FIG. 33 - ISOLINES OF PRESSURE - TEST 6

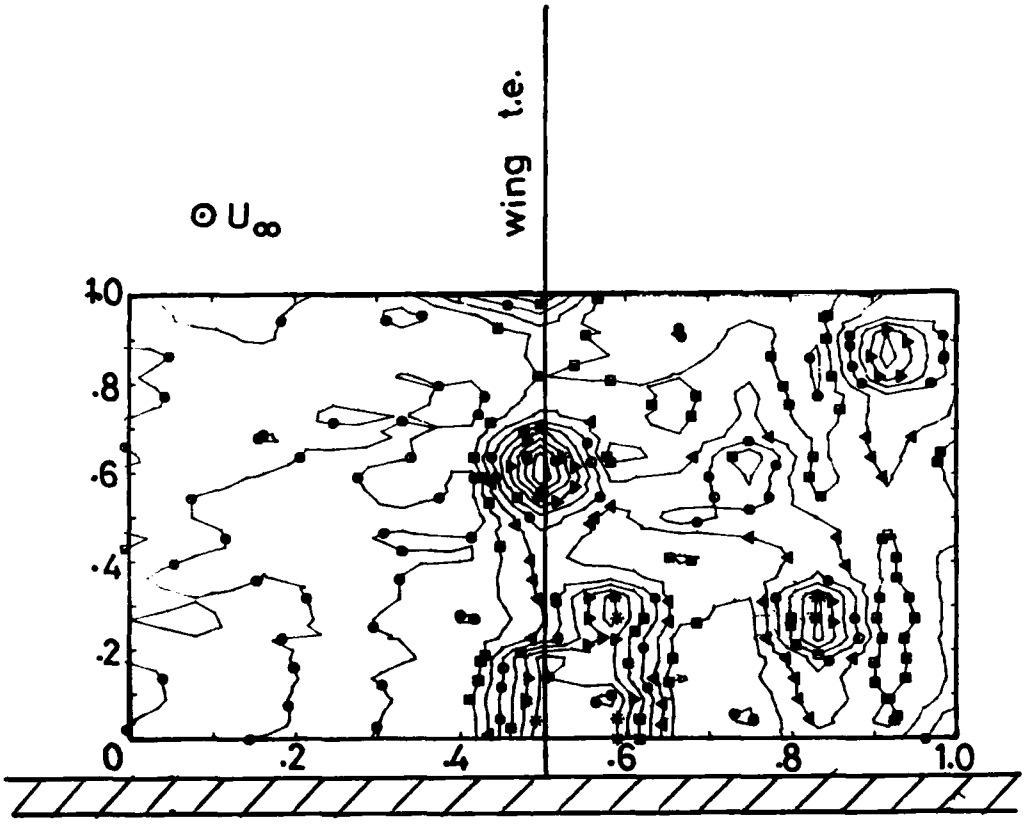

Flat plate

Traverse plane dimensions
60 mm × 110 mm

Velocity = 28 m/s

FIG. 34 - ISOLINES OF PRESSURE - TEST 7

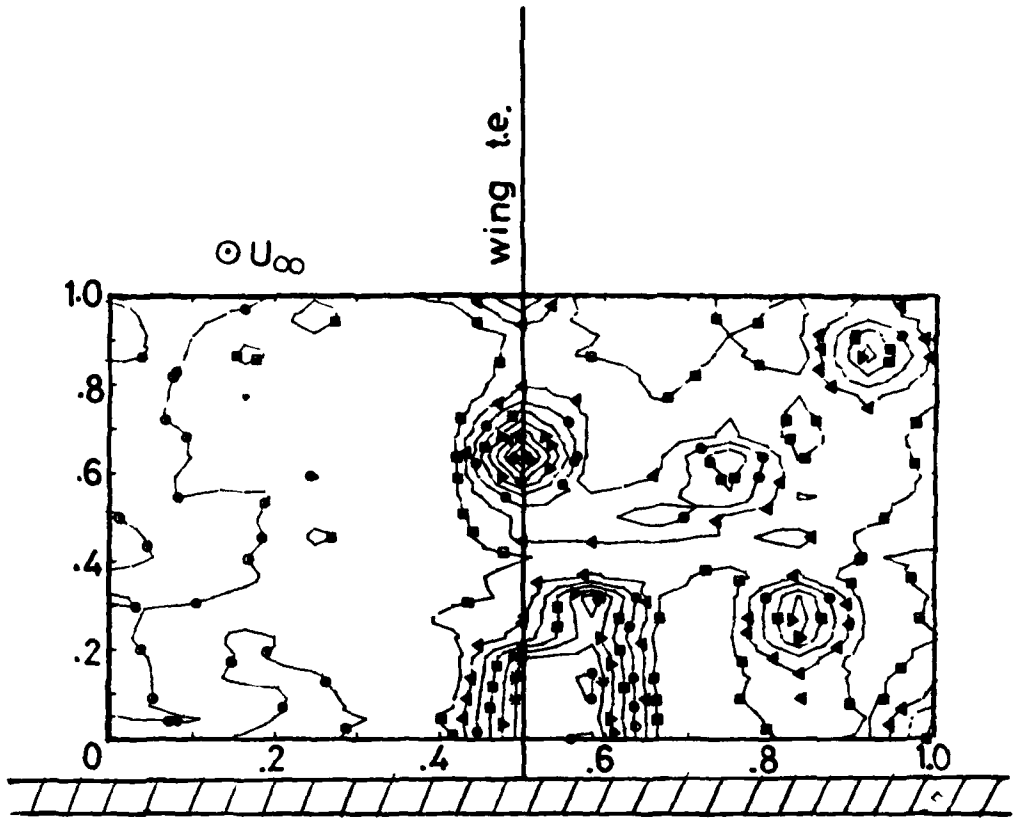

Flat plate

Traverse plane dimensions
60 mm × 110 mm

Velocity = 28 m/s

FIG. 35 - ISOLINES OF PRESSURE - TEST 9

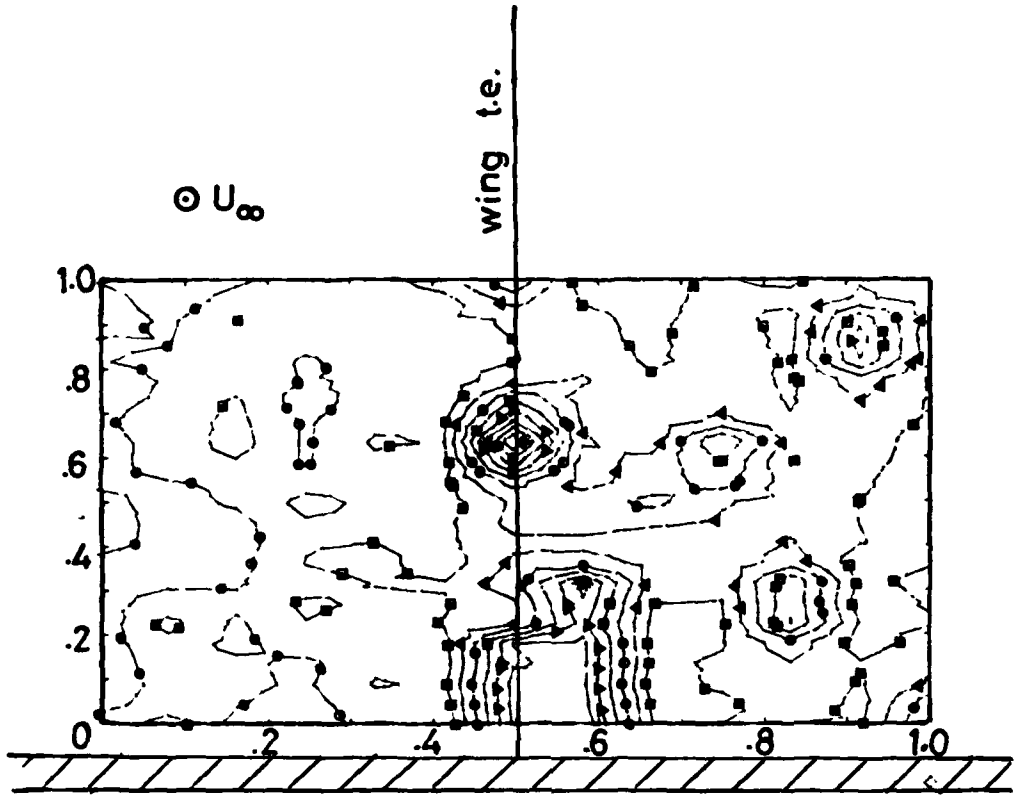

Flat plate

Traverse plane dimensions
60 mm × 110 mm

Velocity = 28 m/s

FIG. 36 - ISOLINES OF PRESSURE - TEST 10

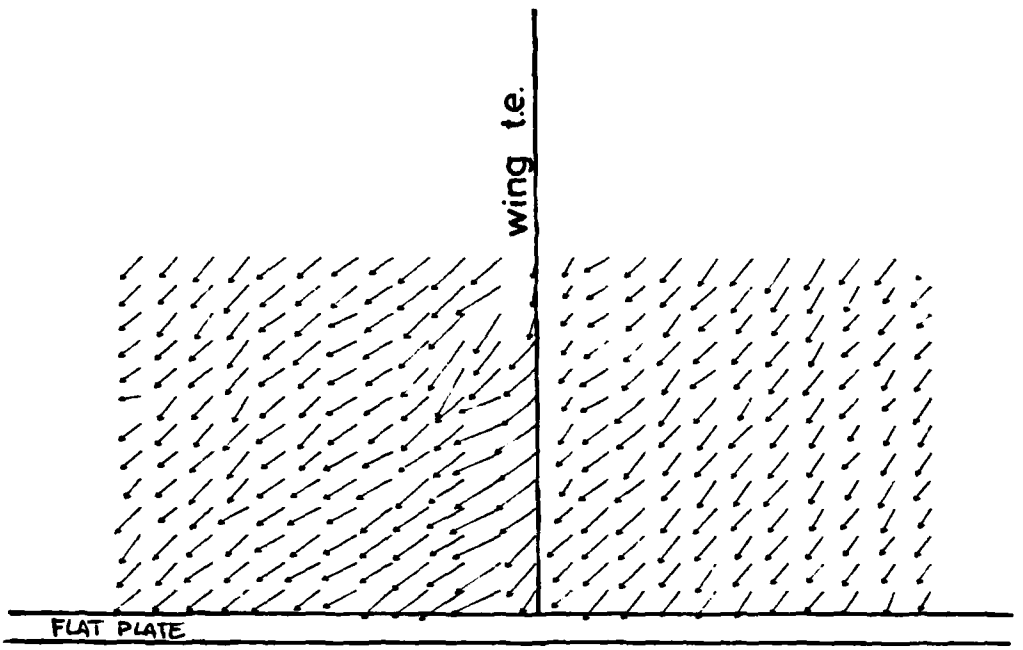

(a) Original version

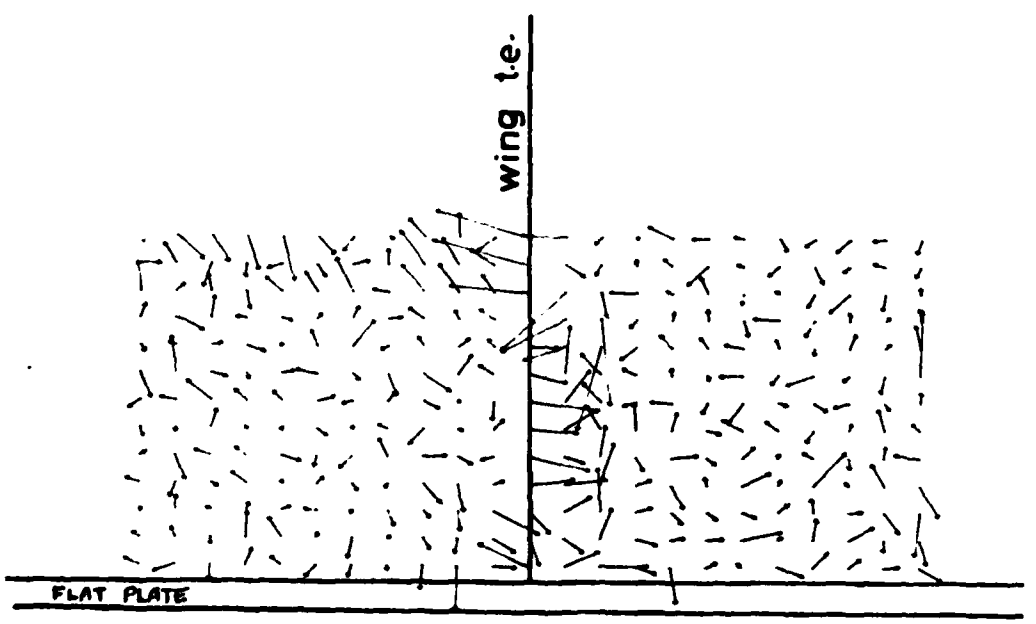

(b) Corrected for downwash

FIG. 37 - SECONDARY VELOCITY v,ω PLOTS

END

DATE
FILMED

5 84

END

DATE
FILMED

5 84

DTIC